NATIONAL BUREAU OF STANDARDS REPORT

9875

THERMAL CONDUCTANCE OF SOILS

Interim Report

Report to

U. S. Atomic Energy Commission
Albuquerque, New Mexico

<NBS>

U.S. DEPARTMENT OF COMMERCE

NATIONAL BUREAU OF STANDARDS

NATIONAL BUREAU OF STANDARDS

The National Bureau of Standards[1] was established by an act of Congress March 3, 1901. Today, in addition to serving as the Nation's central measurement laboratory, the Bureau is a principal focal point in the Federal Government for assuring maximum application of the physical and engineering sciences to the advancement of technology in industry and commerce. To this end the Bureau conducts research and provides central national services in three broad program areas and provides central national services in a fourth. These are: (1) basic measurements and standards, (2) materials measurements and standards, (3) technological measurements and standards, and (4) transfer of technology.

The Bureau comprises the Institute for Basic Standards, the Institute for Materials Research, the Institute for Applied Technology, and the Center for Radiation Research.

THE INSTITUTE FOR BASIC STANDARDS provides the central basis within the United States of a complete and consistent system of physical measurement, coordinates that system with the measurement systems of other nations, and furnishes essential services leading to accurate and uniform physical measurements throughout the Nation's scientific community, industry, and commerce. The Institute consists of an Office of Standard Reference Data and a group of divisions organized by the following areas of science and engineering:

> Applied Mathematics—Electricity—Metrology—Mechanics—Heat—Atomic Physics—Cryogenics[2]—Radio Physics[2]—Radio Engineering[2]—Astrophysics[2]—Time and Frequency.[2]

THE INSTITUTE FOR MATERIALS RESEARCH conducts materials research leading to methods, standards of measurement, and data needed by industry, commerce, educational institutions, and government. The Institute also provides advisory and research services to other government agencies. The Institute consists of an Office of Standard Reference Materials and a group of divisions organized by the following areas of materials research:

> Analytical Chemistry—Polymers—Metallurgy — Inorganic Materials — Physical Chemistry.

THE INSTITUTE FOR APPLIED TECHNOLOGY provides for the creation of appropriate opportunities for the use and application of technology within the Federal Government and within the civilian sector of American industry. The primary functions of the Institute may be broadly classified as programs relating to technological measurements and standards and techniques for the transfer of technology. The Institute consists of a Clearinghouse for Scientific and Technical Information,[3] a Center for Computer Sciences and Technology, and a group of technical divisions and offices organized by the following fields of technology:

> Building Research—Electronic Instrumentation — Technical Analysis — Product Evaluation—Invention and Innovation— Weights and Measures — Engineering Standards—Vehicle Systems Research.

THE CENTER FOR RADIATION RESEARCH engages in research, measurement, and application of radiation to the solution of Bureau mission problems and the problems of other agencies and institutions. The Center for Radiation Research consists of the following divisions:

> Reactor Radiation—Linac Radiation—Applied Radiation—Nuclear Radiation.

[1] Headquarters and Laboratories at Gaithersburg, Maryland, unless otherwise noted; mailing address Washington, D. C. 20234.
[2] Located at Boulder, Colorado 80302.
[3] Located at 5285 Port Royal Road, Springfield, Virginia 22151.

NATIONAL BUREAU OF STANDARDS REPORT

THERMAL CONDUCTANCE OF SOILS

Interim Report

by

D. R. Flynn and T. W. Watson
Environmental Engineering Section
Building Research Division
Institute for Applied Technology

◇NBS◇

U.S. DEPARTMENT OF COMMERCE

NATIONAL BUREAU OF STANDARDS

Thermal Conductance of Soils

Interim Report

D. R. Flynn and T. W. Watson
Institute for Applied Technology
National Bureau of Standards
Washington, D.C. 20234

Abstract

An apparatus is described which has been designed and built to
enable measurement of the thermal conductance of soils at hot face
temperatures approaching 1700 °C. The method utilizes radial heat
flow through a hollow cylinder of soil contained between a central
ceramic core and an outer water-cooled metal shell. Apparent thermal
conductivity values are reported for nine natural or artificial soils
representative of subsoils found on most of the earth's surface. For
four of these soils, measurements have been completed on two different
specimens.

Key Words: Conductance, conductivity, heat transfer, nuclear
safety, soils, temperature, thermal conductance,
thermal conductivity.

1. Introduction

In conjunction with safety evaluation of space nuclear power systems, it is desired to be able to predict the maximum steady-state temperature which will be reached by a given nuclear power supply after reentry impact burial in earth. In order to do this it is necessary to have information regarding the thermal conductance of soils under conditions in which heat flows from a source which may be as hot as 1700 °C to a sink at ambient temperatures.

2. Purpose and Scope

Contract No. ASB48-6179 encompasses an experimental study to measure the effective thermal conductance, as a function of temperature, of nine soils (natural and artificial) selected and furnished by Sandia Corporation. Test temperatures shall be from room temperature to just below the molten range for each soil, with a maximum as near 1700 °C as possible wherever the melt range level permits. Duplicate runs shall be made on each type of soil using different samples.

The thermal conductance shall be measured in a manner that simulates a heat source buried in soil. Artificial gas pressure or inert gas shall not be used in these measurements. Application of any compaction load to the soil samples during test is not allowed.

3. Soil Samples

Samples of the following nine soils selected by Sandia Corporation have been received at the National Bureau of Standards:

1. Calcareous Soil (natural weathered limestone)

2. Granitic Detrital Soil (weathered decomposed granite soil)

3. Dune Sand (windblown sand)

4. Magnesian Soil (magnesium aluminum silicate)

5. Podzol Soil (leached organic timberland soil)

6. Coastal Plains Clay (coastal flood plain soil)

7. Laterite Soil (tropical rain forest soil)

8. Estancia Playa (Dog Lake) Soil (highly saline playa soil)

9. Ottawa Sand (silica-artificial soil)

All of these soils were screened to a maximum particle diameter of 1/16 inch (0.16 cm) prior to shipment to NBS.

Sandia has provided us with detailed information concerning each soil sample. These data include theoretical estimates of solid-state reaction temperatures and reaction magnitudes and of the melt range for each soil to be tested. In order to experimentally investigate the soil melt ranges, significant reaction temperatures, and rates and magnitudes of reactions, differential thermal analyses (DTA) of each soil sample were carried out by the Analytical Coordination Chemistry Section of the NBS Analytical Chemistry Division. The soil sample characterizations supplied by Sandia Corporation and the results of the NBS DTA determinations are given in Appendices A and B.

4. Method and Apparatus for Thermal Conductance Measurements

4.1. Philosophy of Approach

Our prime concern in deciding on the best experimental approach to this problem was to simulate as closely as possible the conditions which a buried heat source would experience. The following considerations apply:

a. The maximum steady-state temperature, T_m (°C), at the surface of a heat source which is surrounded by soil or other material is given by

$$T_m = T_s + \frac{FQ}{\lambda^*} \quad , \tag{1}$$

where T_s (°C) is the temperature of the sink to which heat is lost. The quantity Q (W/m^2) is the power output per unit area from the source. The geometrical factor, F, depends on the spatial configuration of the heat source and sink. The mean thermal conductivity, λ^* (W m^{-1} °C^{-1}), is defined by

$$\lambda^* = \lambda^* (T_s, T_m) = \frac{1}{T_m - T_s} \int_{T_s}^{T_m} \lambda (T) \, d T \, , \tag{2}$$

where $\lambda (T)$ is the temperature-dependent thermal conductivity of the soil. From this we see that it is not necessary to measure the actual thermal conductivity, $\lambda (T)$, as a function of temperature if the mean thermal conductivity, $\lambda^* (T_s, T_m)$, can be measured directly as a function of the hot side temperature. This can be done by measuring T_m as a function of Q for some configuration having a known geometrical factor, F, and then computing λ^* using eq. (1).

3

b. If $\lambda^*(T_s, T_m)$, rather than $\lambda(T)$, is measured, the cold surface of the specimen can be kept at room temperature thus considerably simplifying the problem of containment.

c. If $\lambda(T)$ is desired, it can be computed from measured values of $\lambda^*(T_s, T_m)$.

d. Since the quantity of prime interest is the maximum temperature attained by the buried radio-active source, the values of λ^* which are appropriate are those obtained after monotonic heating of the hot surface of the specimen.

e. The specimen size should be large enough that the heat flow path is much larger than the average particle size of the soil. For a maximum particle diameter of 1/16 inch (0.16 cm), it would seem appropriate for the sample to be at least 1 inch (2.5 cm) thick from the hot surface to the cold surface. Similarly, the heat source in contact with the specimen should be large in comparison with the average particle size of the soil. This would preclude the use of "hot-wire" methods.

f. Since the final steady-state temperature at the source surface is of principal concern, it would not be appropriate to attempt to derive thermal conductivity values from measured values of thermal diffusivity and specific heat. This is particularly so for materials such as soils which are subject to decomposition, phase changes, moisture migration, and other phenomena involving heat generation or absorption.

g. However, it must be realized that a buried source may experience

transient temperatures which are higher than the final steady-

state temperature at the source after equilibrium is attained.

This is so because the thermal conductivity may increase, e.g.,

due to sintering, with time at any given temperature. The best

way to determine what would be the maximum transient temperature

rise at the surface of a buried heat source of strength per unit

area, $Q(W/m^2)$, would be by direct measurement of the temperature-

time relationship in an experiment which closely simulates the

conditions which a heat source buried in soil would encounter.

4.2. Method & General Mathematical Analysis

It was decided to measure the thermal conductance of the soil samples

using the method of radial heat flow in a right circular cylinder. A

cross section of the apparatus is shown in figure 1. The specimen is con-

tained within the annular space between the outer radius, a, of a ceramic

core and the inner radius, b, of a brass shell. A measured quantity of

heat per unit time generated electrically in the ceramic core flows radially

through the specimen to the inner concentric water-cooled brass shell.

The ceramic core has a concentric ring of equally spaced holes at a radius,

r', parallel to the axis, each containing a heater wire. Temperatures

are measured by an axial thermocouple in the ceramic core and by thermo-

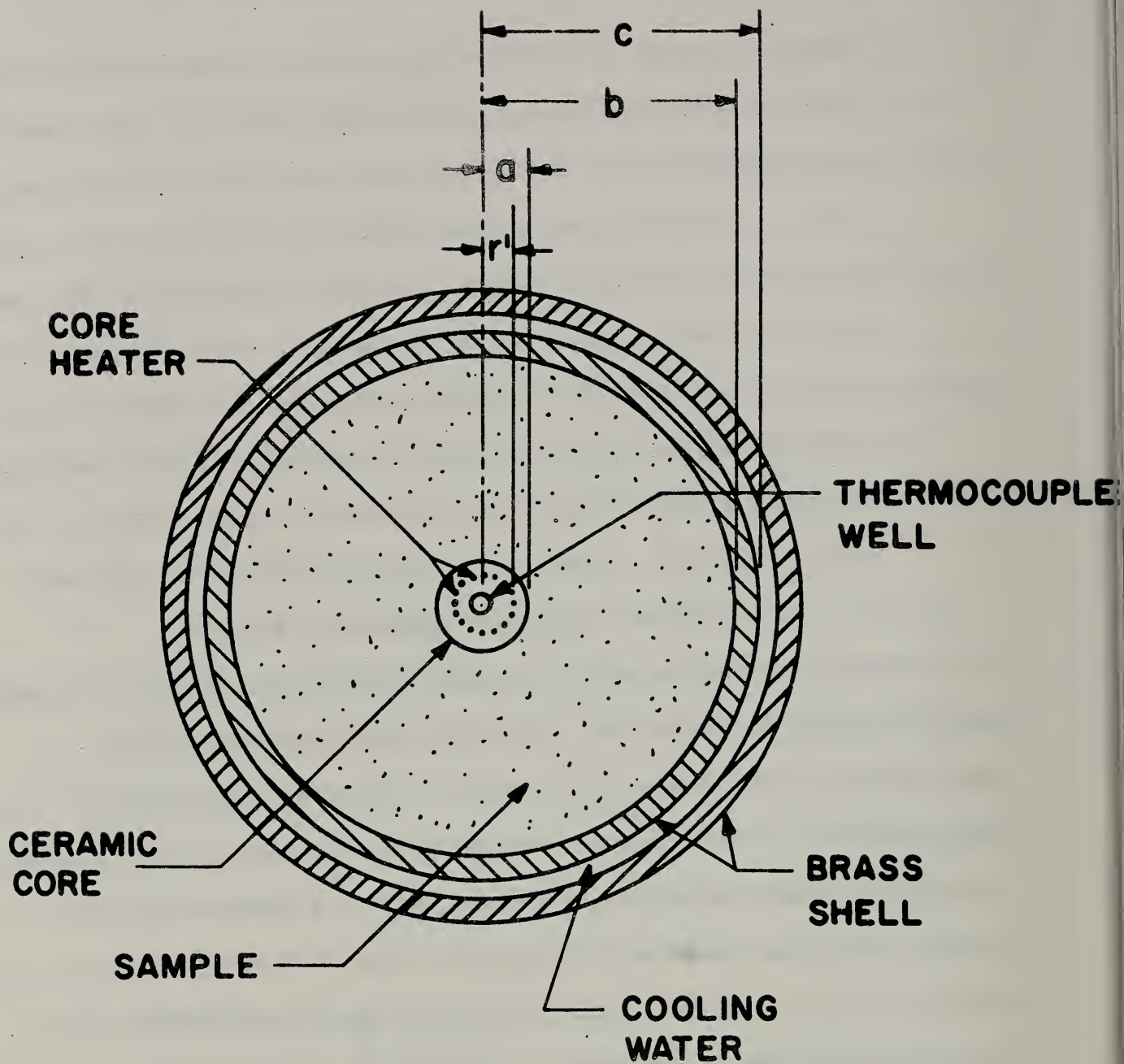couples attached to the outer surface of the inner brass shell at radius c.

5

Figure 1.   Horizontal cross section of the apparatus for measuring the thermal conductance of soils.

In figure 1, if the cylindrical surfaces r = a and r = b are each isothermal, the heat flow between these surfaces will be radial except near the ends of the apparatus. In general, the thermal conductivity of the specimen material will vary with temperature, and the heat flow rate per unit area through a cylindrical element of the sample is

$$-\lambda(T)\frac{dT}{dr} = \frac{Qa}{r} \quad , \tag{3}$$

where temperature is denoted by the symbol T and the temperature-dependent thermal conductivity by $\lambda(T)$. If eq. (3) is rearranged and integrated, we obtain

$$\int_{T_b}^{T_a} \lambda(T)dT = Qa\ell n(b/a) \quad , \tag{4}$$

where T_a and T_b are the temperatures at r = a and r = b respectively. Let us define a mean thermal conductivity $\lambda^*(T_b, T_a)$ over the temperature range T_b to T_a:

$$\lambda^*(T_b, T_a) = \frac{1}{T_a - T_b} \int_{T_b}^{T_a} \lambda(T)dT \quad . \tag{5}$$

Combining eqs. (4) and (5), we obtain

$$\lambda^*(T_b, T_a) = \frac{Qa\ell n(b/a)}{T_a - T_b} \tag{6}$$

as the expression which can be used to compute λ^* from measurable quantities.

7

As an example of the use of (6) let us consider the case where the thermal conductivity of the sample can be assumed to vary linearly with temperature:

$$\lambda(T) = \lambda_0 [1 + \alpha_0 (T - T_0)] \quad , \tag{7}$$

where λ_0 is the thermal conductivity at an arbitrary reference temperature, T_0, and α_0 is the corresponding temperature coefficient of thermal conductivity. Substitution of (7) into (5) yields, after integration,

$$\lambda^*(T_b, T_a) = \lambda_0 \left[1 + \alpha_0 \left(\frac{T_a + T_b}{2} - T_0 \right) \right] = \lambda \left(\frac{T_a + T_b}{2} \right) \quad . \tag{8}$$

Thus, for a material for which the thermal conductivity varies linearly with temperature, eq. (6) yields a thermal conductivity corresponding to the average of the temperatures at the hot and cold surfaces of the sample.

Equation (6) requires a knowledge of the temperatures T_a and T_b at the inner and outer surfaces of the sample. Experimental difficulties (e.g., finite size of temperature sensors and contamination of sensors by the sample) preclude direct measurement of T_a and T_b. Reference to figure 1 shows that there are four temperature drops which must be considered in deriving T_a and T_b from the measured temperatures:

1. The temperature drop between the thermocouple well in the center of the ceramic core and the surface, r = a, of the ceramic core.

2. The temperature drop due to the thermal contact resistance between the surface of the ceramic core and the inner surface of the sample, both surfaces being nominally at r = a.

3. The temperature drop due to the thermal contact resistance between the outer surface of the sample and the inner surface of the brass shell, both surfaces being nominally at r = b.

4. The temperature drop between the inner surface, r = b, of the brass shell, and the outer surface, r = c, where the temperature is measured.

If the circle of heater wires at r = r' were a continuous cylindrical heat source, the entire region r < r' inside the heater circle would be isothermal. For the case of a finite number of line heat sources at r = r', the temperature measured at the axis is equal to the average temperature, T_h, at the radius of the heater circle [1,2].[1] Therefore the temperature drop between the thermocouple well in the center of the core and the surface of the core is given by

$$T_h - T_a' = \frac{Qa \ln(a/r')}{k_c} \, , \qquad (9)$$

where k_c is the thermal conductivity of the ceramic core material and T_a' is the temperature at the outer surface, r = a, of the ceramic core (as opposed to T_a, which is the temperature at the inner surface, also r = a, of the sample).

---

[1] Figures in brackets indicate the literature references at the end of this report.

If we designate R_a as the thermal contact resistance per unit area ($^\circ$C m^2 W^{-1}) at the core specimen interface ($r = a$), then the temperature drop across this interface is given by

$$T_a' - T_a = R_a Q \quad . \tag{10}$$

Similarly, the temperature drop at the specimen-shell interface ($r = b$) is given by

$$T_b - T_b' = \frac{a}{b} R_b Q \quad , \tag{11}$$

where T_b' is the temperature at the inner surface, $r = b$, of the brass shell (as opposed to T_b, which is the temperature at the outer surface, also $r = b$, of the sample) and R_b is the thermal contact resistance per unit area at the specimen-shell interface.

The temperature drop across the brass shell is

$$T_b' - T_c = \frac{Qa\ell n(c/b)}{k_s} \quad , \tag{12}$$

where T_c is the temperature at the outer surface of the shell, $r = c$, and k_s is the thermal conductivity of the shell material.

In the apparatus configuration shown in figure 1, the temperatures measured correspond to T_h and T_c as defined above. Combining equations (6), and (9) through (12), we can eliminate all of the temperatures involved except T_h and T_c and thus obtain, instead of (6),

$$\lambda^*(T_b, T_a) = \frac{Qa\,\ell n(b/a)}{T_h - T_c} \left[1 - \frac{Qa}{T_h - T_c} \left(\frac{\ell n(a/r')}{k_c} + \frac{\ell n(c/b)}{k_s} + \frac{R_a}{a} + \frac{R_b}{b} \right) \right]^{-1} . \tag{13}$$

The magnitude of the correction terms in eq. (13) is more readily seen if we define

$$\lambda^*_{app} = \frac{Qa \ \ell n(b/a)}{T_h - T_c} \qquad (14)$$

as the apparent value of thermal conductivity obtained by neglecting the correction terms; combining (13) and (14) we obtain

$$\lambda^*(T_b,T_a) = \lambda^*_{app} \left[1 - \frac{\lambda^*_{app}}{\ell n(b/a)} \left(\frac{\ell n(a/r')}{k_c} + \frac{\ell n(c/b)}{k_s} + \frac{R_a}{a} + \frac{R_b}{b} \right) \right]^{-1} \qquad (15)$$

Equation (15) is the basic equation to be used for calculating mean thermal conductivity values if the heat is assumed to flow radially. The quantities a, b, Q, T_h, and T_c involved in the definition of λ^*_{app} (eq. (14)) are all directly measurable. The quantities k_c, k_s, R_a, and R_b (required for the correction terms in (15)) must either be known or the corresponding correction terms shown to be negligible.

4.3. Longitudinal Heat Flow

The analysis given above is based on the assumption of purely radial heat flow in the alumina core and in the specimen. Owing to the finite length of the apparatus, consideration must be given to the effects of longitudinal heat flow in the core and in the specimen.

Peavy [2] has considered the effect of longitudinal heat flow in an apparatus such as that used in the present investigation. His analysis is exact for the case in which both the core and the specimen have constant thermal conductivity and the heat generation per unit length does not vary along the core. Flynn [1] has considered the effect of longitudinal heat flow along the core for the case in which the heat generation per unit length is a linear function of temperature. His analysis neglects

11

longitudinal heat flow in the specimen and assumes a constant thermal conductivity (i.e., independent of temperature) for the core.

In the present investigation the very large temperature differences within the apparatus make it imperative that the temperature dependence of the thermal conductivity of the core, the temperature dependence of the thermal conductivity of the specimen, and the temperature dependence of the heat generation per unit length all be taken into account. Peavy's analysis [2] would be very difficult to adapt to the case in which all these parameters have large temperature dependences. Flynn's analysis [1] can easily be modified to include the effect of the temperature dependence of the thermal conductivity of the core and with a little more effort be extended to include a more complicated (than linear) temperature dependence for the heat generation per unit length in the core. However, his analysis is inherently incapable of dealing with the effects of longitudinal heat flow in the specimen.

Since the apparatus design permits direct experimental measurement of the temperature distribution along the axis of the core, we have more information than is available in boundary value problems in which only the conditions on the outside of the system are prescribed. This additional information enables us to compute the effects of longitudinal heat flow in a rather straightforward manner with only minor approximations being required. If necessary even these approximations could be circumvented by a simple process of iteration.

Let us first consider the situation which exists in the alumina core.
The thermal conductivity of high-density, high-purity alumina decreases
by a factor of more than six between room temperature and 1600 °C. The
electrical resistivity of the 60% Pt - 40% Rh alloy used for the heater
winding increases by a factor of three between room temperature and
1600 °C. Both the thermal conductivity of the core and the electrical
resistivity of the heater (and hence the heat generation per unit length)
are explicit functions of temperature. Since we experimentally measure
the temperature distribution along the axis of the core and since the
temperature at the axis of the core is essentially the same as the
temperature of the heater winding, we can determine the thermal conductivity
of the core (inside the circle of heater wires) and the heat generation
per unit length as functions of position. For a given test we can treat
both of these quantities as if they were explicit functions of position.

Consider an element of the core of length dz. The heat generated
in this element is $mI^2\beta dz$, where m is the number of heater wires, I is
the electric current flow through the heater winding, and β is the
electrical resistance per unit length of heater wire. The radial heat
flow from the convex surface of this element into the specimen is
$2\pi aQdz$, where now $Q = Q(z)$ varies with longitudinal position. The heat
flowing into this element in the positive z-direction is $-C(d\bar{v}/dz)$, where
C is the ("position-dependent") thermal conductance of the core,

13

including heater wires, and $\bar{v}$ is the average temperature of the core at longitudinal position z. The heat leaving the element in the positive z-direction is

$$-C(d\bar{v}/dz) + (d/dz)[-C(d\bar{v}/dz)]dz.$$

Under steady-state (i.e. temperature independent of time) conditions, conservation of energy enables us to write

$$\frac{d}{dz}\left(C\,\frac{d\bar{v}}{dz}\right) - 2\pi a Q(z) = -mI^2\beta(z) \tag{16}$$

as the differential equation relating $\nabla(z)$, $Q(z)$, and $\beta(z)$. If $\bar{v}$ and β are known or measured, the heat flux into the specimen at any longitudinal position is

$$Q(z) = \frac{1}{2\pi a}\left[mI^2\beta + \frac{d}{dz}\left(C\,\frac{d\bar{v}}{dz}\right)\right]. \tag{17}$$

Mathematically, the average core temperature at any longitudinal position is given by

$$\bar{v}(z) = \frac{2}{a^2}\int_0^a rv(r,z)\,dr. \tag{18}$$

With this definition of $\bar{v}$, eq. (17) is completely rigorous.

Except very near the ends of the apparatus, most of the heat flow in the core is radial rather than longitudinal. Hence, to a good approximation, the temperature at any position in the core is given by

$$v(r,z) = \begin{cases} v(0,z) & , \ 0 < r < r' \\ v(0,z) - \dfrac{mI^2\beta}{2\pi}\displaystyle\int_{r'}^{r}\frac{1}{k_c}\frac{dr}{r} & , \ r' < r < a \end{cases}, \tag{19}$$

14

where $v(0,z)$ is the experimentally determined temperature distribution along the axis of the core. Substituting this expression into (18), the average temperature of the core at any cross section is given very closely by

$$\bar{v}(z) = v(0,z) - \frac{mI^2\beta}{\pi a^2} \int_{r'}^{a} r\, dr \int_{r'}^{r} \frac{1}{k_c} \frac{dr}{r} \quad . \tag{20}$$

For the relatively small radial temperature differences between $r = r'$ and $r = a$ we can justifiably neglect the temperature dependence of k_c and thereby reduce (20) to

$$\bar{v}(z) = v(0,z) - \frac{mI^2\beta}{\pi a^2 k_c} \int_{r'}^{a} r\, \ell n\, \frac{r}{r'}\, dr$$

$$= v(0,z) - \frac{mI^2\beta}{4\pi k_c} \left[2\ell n\, \frac{a}{r'} - 1 + \frac{r'^2}{a^3} \right] \quad . \tag{21}$$

This equation can be substituted into (17) to enable calculation of $Q(z)$, the radial heat flux into the specimen at all longitudinal positions.

By writing a differential equation (eq. (16)) in terms of $\bar{v}$, the average core temperature, we were able to determine the heat flux, $Q(z)$, into the inner surface, $r = a$, of the specimen. We now show the analysis needed to permit computation of the thermal conductivity of the specimen. Consider an apparatus, having the horizontal cross section shown in figure 1, which is of finite length, extending from $z = 0$ to $z = \ell$, with the flat ends water cooled. We define $v = 0$ at $r = b$, neglect contact resistances, and write the boundary conditions for the specimen as

$$a < r \leq b \qquad z = 0 \text{ and } z = \ell \qquad v = 0 \quad ,$$

$$r = b \qquad 0 \leq z \leq \ell \qquad v = 0 \quad , \tag{22}$$

$$r = a \qquad 0 < z < \ell \qquad -\lambda(v)\, \frac{\partial v}{\partial r} = Q(z) \quad .$$

15

In order to simplify the boundary condition at the surface of the core, $r = a$, we introduce a new variable defined by

$$y = \frac{1}{\lambda_0} \int_0^V \lambda(v) dv = \frac{\lambda^*(v)}{\lambda_0} \, v \quad , \tag{23}$$

where $\lambda_0 = \lambda(v = 0)$. In terms of y, the boundary conditions, (22), can be written as

$a < r \leq b$	$z = 0$ and $z = \ell$	$y = 0$	,
$r = b$	$0 \leq z \leq \ell$	$y = 0$	,
$r = a$	$0 < z < \ell$	$-\lambda_0 \frac{\partial y}{\partial r} = Q(z)$.	

(24)

With these boundary conditions, the solution of the Laplacian equation for the potential, y, is given by Carslaw and Jaeger [3, p. 221] as

$$y(r,z) = \frac{-1}{\lambda_0} \sum_{n=1}^{\infty} \frac{\ell \, A_n \, F_0(n\pi r/\ell; n\pi b/\ell)}{n\pi \, F_1(n\pi a/\ell; n\pi b/\ell)} \sin \frac{n\pi z}{\ell} \quad , \tag{25}$$

where

$$A_n = \frac{2}{\ell} \int_0^\ell Q(z') \sin \frac{n\pi z'}{\ell} \, dz' \quad , \tag{26}$$

$$F_0(x;y) \equiv I_0(x)K_0(y) - I_0(y)K_0(x) \quad , \tag{27}$$

and

$$F_1(x;y) \equiv I_1(x)K_0(y) + I_0(y)K_1(x) \quad . \tag{28}$$

$I_n(x)$ and $K_n(x)$ being modified Bessel functions of the first and second kind, respectively, and of order n.

Evaluation of (25) at $r = a$ and comparison with (23) enables us to write

$$\lambda^*(v) = \frac{-1}{v(a,z)} \sum_{n=1}^{\infty} \frac{\ell \, A_n \, F_0(n\pi a/\ell; n\pi b/\ell)}{n\pi \, F_1(n\pi a/\ell; n\pi b/\ell)} \sin \frac{n\pi z}{\ell} \, . \tag{29}$$

Since we know that the heat flow will be essentially radial near the center of the apparatus, it is useful to rewrite (29) in the form

$$\lambda^*(v) = \frac{Q(z) \, a \, \ln(b/a)}{v(a,z)} [1 - U(z)] ,\qquad (30)$$

where $U(z)$, a correction term for the effects of longitudinal heat flow in the specimen, is given by

$$U(z) = \frac{1}{Q(z)} \sum_{n=1}^{\infty} A_n \left\{ 1 - \frac{1}{\ln(b/a)} \cdot \frac{\ell}{n\pi a} \frac{F_0(n\pi a/\ell ; n\pi b/\ell)}{F_1(n\pi a/\ell ; n\pi b/\ell)} \right\} \sin \frac{n\pi z}{\ell} . \qquad (31)$$

In deriving eq. (30), we neglected the influence of contact resistances. Since $U(z)$ is a small correction, we assume that it is still valid even if contact resistances are taken into account. Comparing eqs. (14), (15), and (30), we write

$$\lambda^*(T_b, T_a) = \frac{\lambda^*_{app} [1 - U(z)]}{\left[1 - \frac{\lambda^*_{app}}{\ln(b/a)} \left(\frac{\ln(a/r')}{k_c} + \frac{\ln(c/b)}{k_s} + \frac{R_a}{a} + \frac{R_b}{b} \right) \right]} , \qquad (32)$$

where λ^*_{app} now has the more general definition

$$\lambda^*_{app} = \frac{Q(z) \, \ln(b/a)}{T_h - T_c} , \qquad (33)$$

where $Q(z)$ is given by eq. (17). Equation (32) is the equation used in the present investigation to compute λ^*.

17

4.4. Apparatus

A vertical cross section of the apparatus designed and built for the thermal conductance measurements is shown in figure 2. The specimen is contained in the annular space between the central ceramic core, which is supported at both ends, and the inner brass shell. Cooling water flows in the 3-mm annulus between this inner brass shell and a coaxial outer brass shell.

The central core is an extruded alumina rod, 46 cm long and 1.25 cm in diameter. A horizontal cross-section of this core is shown in figure 3. Sixteen equally-spaced holes, 0.09 cm in diameter, extend the entire length of the rod. The centers of these holes form a circle of 0.44 cm radius. The core heater, which provides the heat flowing radially through the specimen, consists of lengths of platinum-40 percent rhodium (0.06 cm diameter) wire threaded back and forth through the sixteen holes. The core is held from beneath by a ceramic insulating support designed to permit free expansion of the heater wire. The upper end of the core passes through a hole in the removable flange at the top of the apparatus; this hole is a sufficiently loose fit to permit free expansion of the core. Current leads and voltage taps are attached to the heater winding at the upper end of the core.
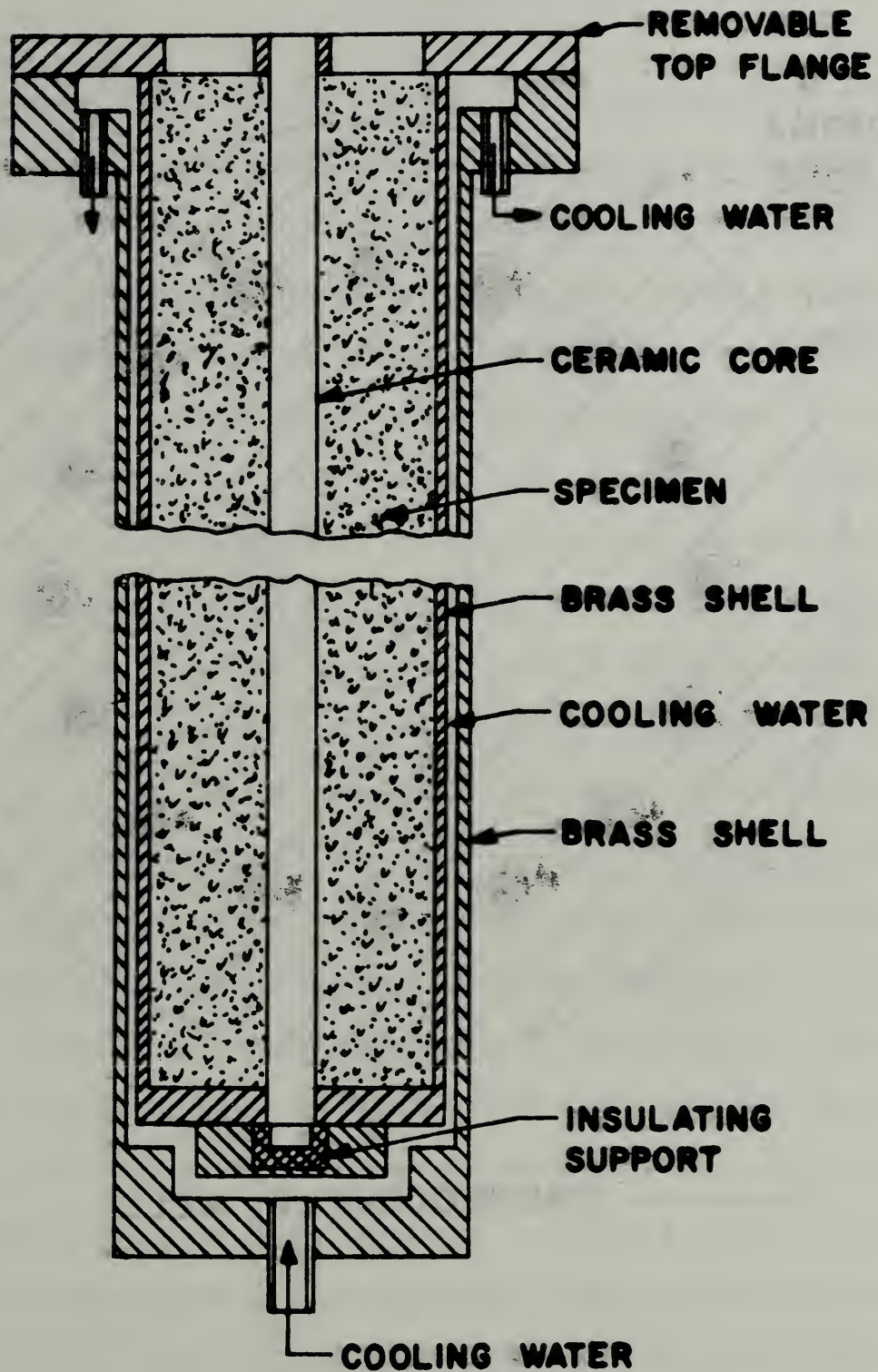
REMOVABLE
TOP FLANGE

COOLING WATER

CERAMIC CORE

SPECIMEN

BRASS SHELL

COOLING WATER

BRASS SHELL

INSULATING
SUPPORT

COOLING WATER

Figure 2.   Vertical cross section of the apparatus for measuring
the thermal conductance of soils.

19

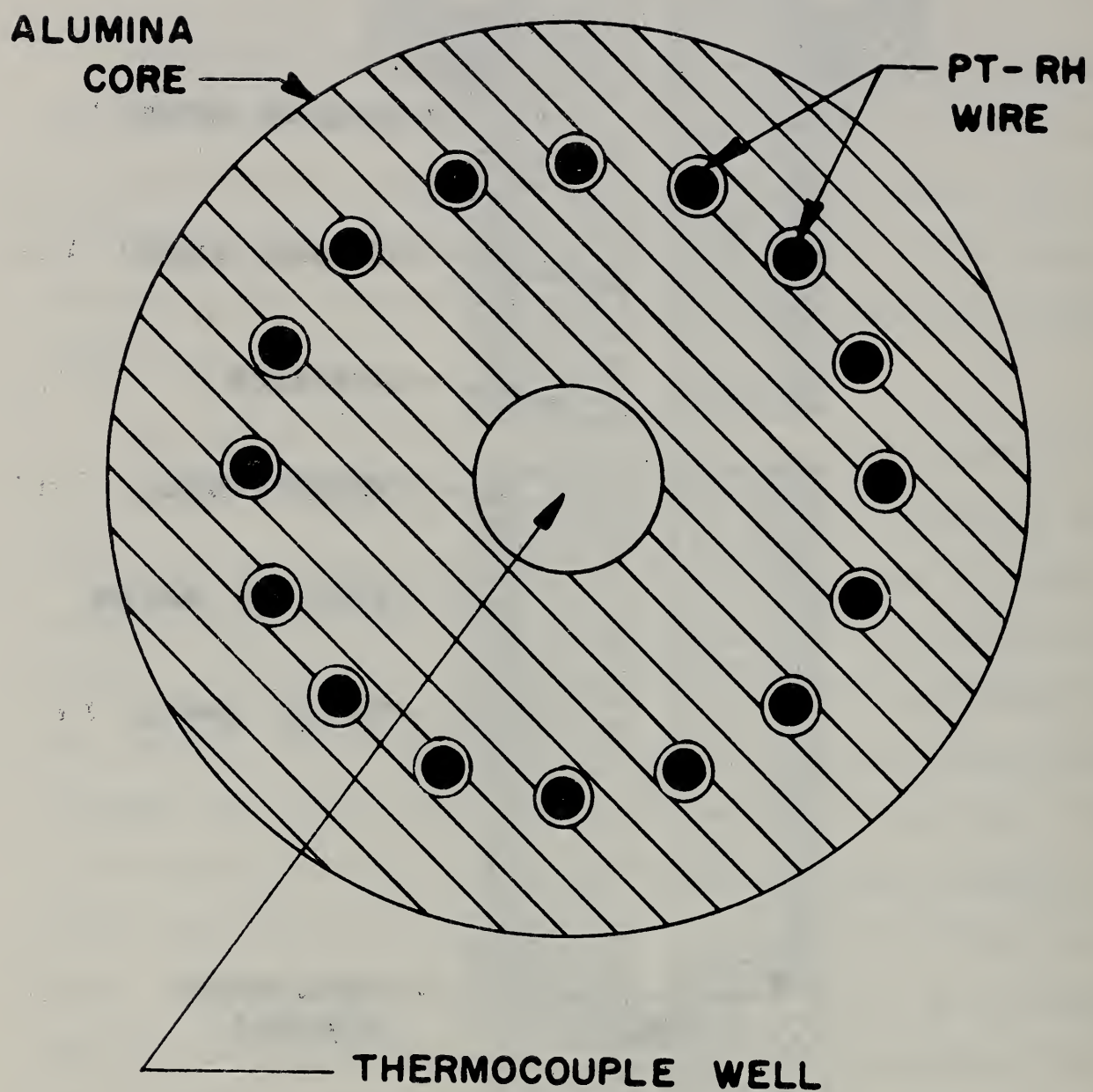ALUMINA
CORE

PT-RH
WIRE

THERMOCOUPLE WELL

Figure 3.   Horizontal cross section of the ceramic core.

In the center of the alumina core there is an axial hole 0.25 cm in diameter. This hole accommodates a thermocouple which can be moved vertically by exterior manipulation. This thermocouple is fabricated from 0.04 cm diameter platinum and platinum - 10 percent rhodium wire and is contained in double-bore alumina tubing which is a snug slip fit in the thermocouple well. The temperature measured at the midlength of the apparatus is designated T_h. This thermocouple can also be utilized to obtain the longitudinal temperature distribution along the core - this information is needed to make corrections for longitudinal heat losses.

With the exception of the ceramic core, all surfaces in contact with the specimen are water-cooled to maintain them at room temperature. As shown in figure 2, the cooling water enters the center of the bottom of the apparatus, passes upward in the annulus between the inner and outer brass shells, and exits at the top of the apparatus. A circulating system, shown in figure 4, is used to maintain a constant temperature in the apparatus. The water leaving the apparatus is pumped through a heat exchanger which cools the water to a temperature lower than that desired at the inlet to the apparatus. From the heat exchanger, the water enters a small commercial hot water heater where it is reheated to the desired temperature for circulation to the apparatus. A resistance thermometer at the exit from the tank is used to control the power to the heater in the tank and thus maintain the desired water temperature.
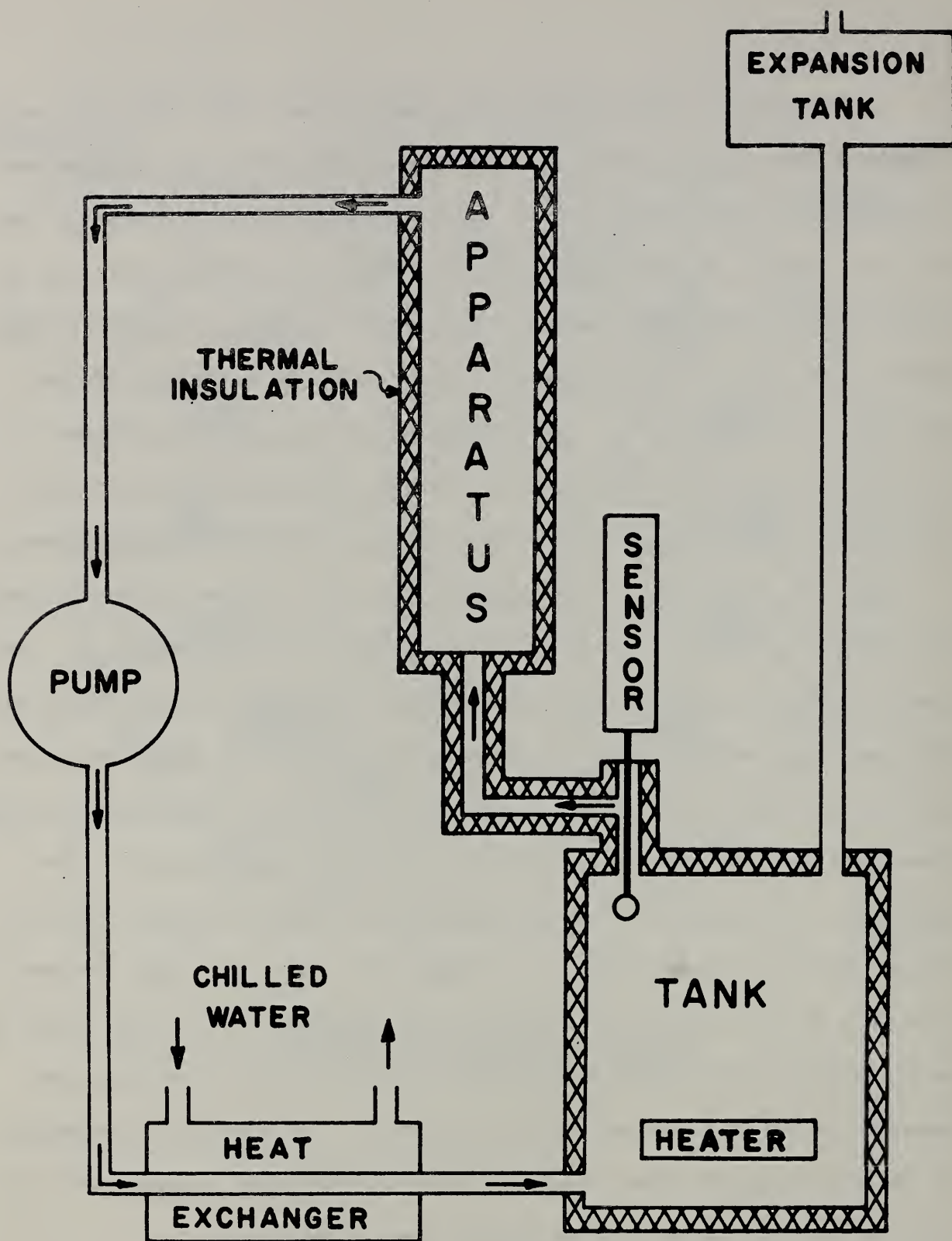
Figure 4.   The circulating system used to cool the apparatus.

Two copper versus constantan thermocouples (0.025 cm diameter) are attached to the outer surface of the inner brass shell at the midplane of the apparatus. The junctions of these thermocouples are thermally insulated from the cooling water by plastic electrical tape. The average of these two temperatures is designated T_c. Additional copper-constantan thermocouples are used to monitor temperatures at different locations in the circulating system.

Individual ice junctions are used with the platinum versus platinum-10 percent rhodium thermocouple used to measure T_h. The constantan leads of the copper versus constantan thermocouples are brought to an isothermal zone box at room temperature. A thermocouple with one junction in the zone box and one in an ice bath is placed in series with a double-pole selector switch, so that each measuring thermocouple is automatically referenced against the ice bath[4].

The ceramic core heater, which provides the heat flowing radially through a specimen, is fed a-c power from a saturable core reactor which is controlled by a current-adjusting-type proportional controller incorporating automatic rate and reset action. This controller has been modified to operate in either of two modes. It can adjust the power to the core heater so as to maintain the temperature, T_h, at the center of the core at a constant value. Alternatively, it can control the saturable core reactor so as to provide constant current to the core heater. The power dissipated in the core heater is determined by measuring the current through the heater and the voltage drop across the heater utilizing one-quarter-percent-accuracy electrodynamic voltmeters and ammeters.

5. Testing Procedure and Calculation Procedure

5.1. Specimen Preparation

Sandia Corporation provided us with desired dry bulk density values
for each of the soil samples supplied. These desired densities were
based on the maximum densities attained in a series of tests using
ASTM Method of Test D698. This test method provides a specified compac-
tion procedure based on dropping a weight a fixed distance a given number
of times. This compaction procedure had been carried out on each soil
for a number of samples having different moisture contents; the moisture
contents which resulted in the highest dry bulk densities were reported
to us.

Adaptation of ASTM D698 to the geometry of our thermal conductivity
apparatus required considerable effort. We were successful in developing
a compaction procedure, based on ASTM D698, which enabled rapid, reliable
compaction of the soil samples with reproducible densities. The bulk
densities obtained with our compaction rig did not always agree with
those densities obtained with ASTM D698 for similar samples at nominally
the same moisture content and compaction energy. We were always able
to come reasonably close to the desired bulk densities with only a few
trials, however.

Each thermal conductivity sample was compacted into a new brass can
(the inner brass shell shown in figure 2). This can had a centered
hole in the bottom which held the lower end of the ceramic core (heater)
coaxially within the can. During the compaction operation, a combination
weight guide and core support, as shown in figure 5, was affixed to the
upper end of the brass can which was to contain the specimen. The core
support held the upper end of the ceramic core (heater) coaxially within
the can during compaction; the core support was spring-loaded to hold
the ceramic core down during compaction. A brass weight was used to
compact the soil in the specimen container. This weight had an outside
diameter slightly smaller than the inside diameter of the specimen
container and was provided with a keyhole-shaped slot to clear the core
support and web shown in figure 5. An attachment extending above the
top of the weight prevented the weight from rotating even when the
weight was totally within the specimen can. The weight guide could be
rotated when desired so that the keyhole-shaped slot in the weight
would not always impinge on the same position of the specimen.

Specimen preparation consisted of the following steps:

1. A small amount of the soil was oven-dried to constant weight
   at 110 °C in order to determine the existing moisture content.
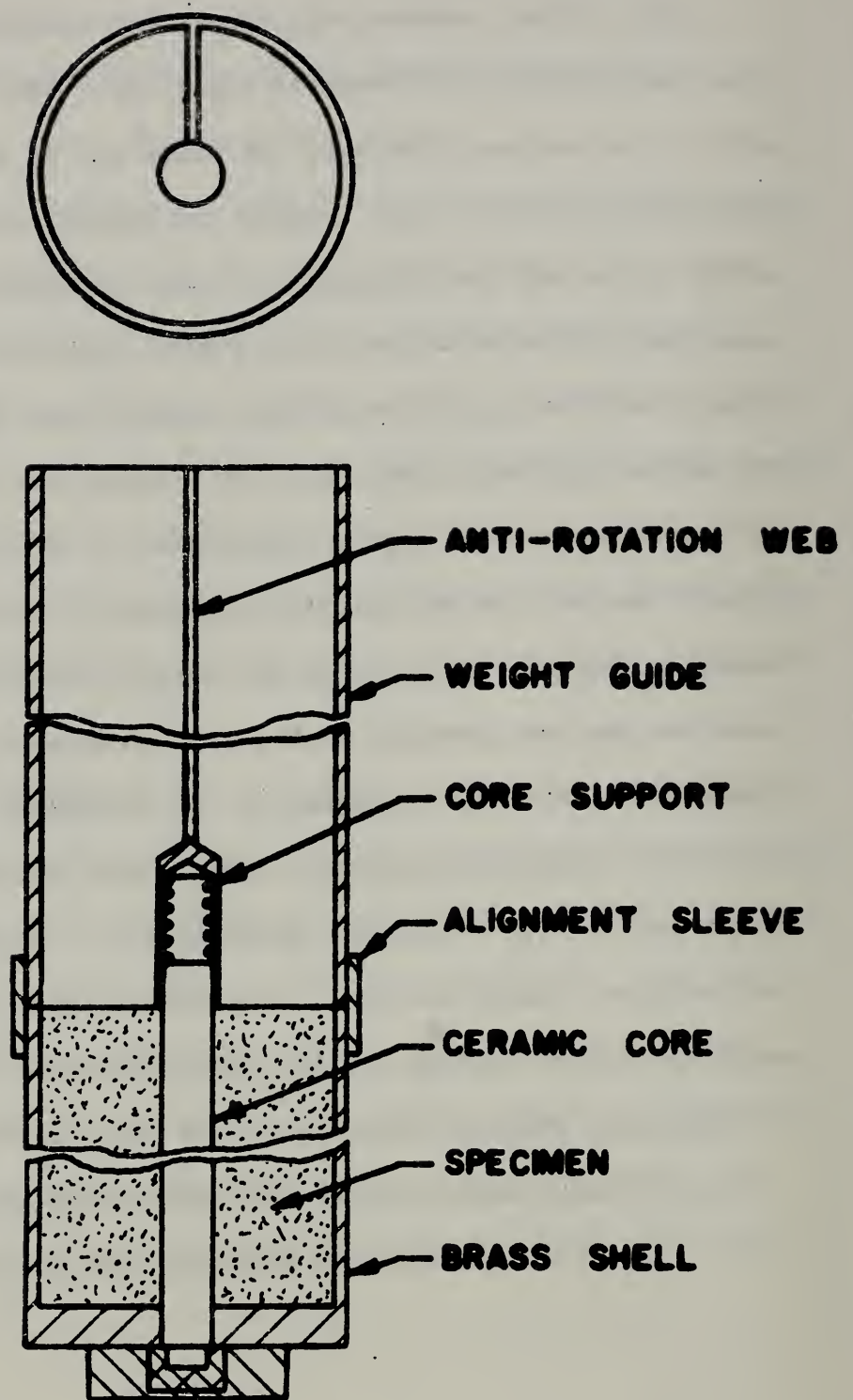
25

Figure 5. Rig used for compacting the soil samples.

2. Meanwhile the brass can (which would later receive the specimen) and the ceramic core (heater) were weighed.

3. Sufficient additional moisture was added to a soil sample to attain the moisture content desired.

4. The compaction rig shown in figure 5 was affixed to the top of the specimen container with the heater centered in place.

5. A mass of moisture-conditioned soil equal to one-tenth of the total mass needed to achieve the desired density was placed in the specimen container.

6. The weight was dropped a fixed distance a given number of times to achieve the desired compaction energy.

7. Another layer of soil was placed in the specimen container and this layer was compacted as above. This procedure was repeated until the specimen container was filled.

8. The filled specimen container was oven-dried to constant weight at 110 °C.

9. The specimen and container were weighed and the specimen dry bulk density was computed.

10. If the dry bulk density obtained was sufficiently close to the desired value, testing proceeded. Otherwise, the specimen was removed and re-packed using a different compaction energy.

A few of the soil samples did not lend themselves to the above compaction procedure. The specimens of Ottawa sand, dune sand, and coastal plains clay were packed to the desired density by filling the specimen container slowly with dry soil while rapping it with a small hammer.

5.2. Testing Procedure

A specimen container, with the ceramic core heater and the compacted specimen installed, was placed in the outer brass shell as shown in figure 2. Rubber O-rings, not shown in figure 2, provided water tight seals at the top of the apparatus. The current leads and voltage taps were attached to the heater leads extending from the top of the ceramic core. A thermocouple was installed in the axial hole in the ceramic core so that the hot junction was at the mid-height of the apparatus. The upper end of this thermocouple was attached to a height gage which permitted moving the thermocouple vertically by known distances.

The circulating system shown in figure 4 was activated to maintain the outside of the specimen container at the desired temperature. This involved adjusting the amount of chilled water passing through the heat exchanger as well as the setting of the temperature controller connected to the resistance bulb in the water tank.

The specimen heater was energized with the proportional controller operating in a constant-temperature mode so as to bring and maintain the temperature at the core thermocouple to the desired value. This procedure effectively prevented significant temperature overshoot, allowing monotonic heating of the hot face of the sample but yet permitting rapid equilibrium to be attained. When the temperature indicated by the core thermocouple was steady and when the electrical power required to maintain this temperature had also leveled out to a steady value, the proportional controller was switched to a constant-current mode so as to maintain the current to the heater at the value it had had before switching over.

After any small disturbances due to mode-changing had had time to die out, several successive readings were taken of the current through the heater, the voltage drop across the heater, the emf of the Pt - 10% Rh: Pt thermocouple (at the mid-height of the apparatus) in the axial hole in the ceramic core, and the emfs of the two copper:constantan thermocouples on the outside of the specimen container. After satisfactory data were obtained with the core thermocouple at the mid-height of the apparatus, the thermocouple junction was moved to a position approximately level with the bottom of the specimen. The emf of the core thermocouple was read at this position and then at approximately 2.5 cm intervals

29

along the entire length of the specimen, time being allowed at each position for the thermocouple junction to reach thermal equilibrium with the ceramic core. The core thermocouple junction was then returned to the mid-height of the apparatus and readings were again taken of the heater current, heater voltage, and thermocouple emfs.

Following completion of one set of data, the heater controller was switched to constant temperature mode and the heater and both controllers were adjusted to bring the specimen to the next condition desired. Data were normally taken at 200 °C intervals to about 1100 °C (hot-side) and then at 100 °C intervals until either the heater burned out or the core thermocouple ceased to function properly.

For the first tests conducted, the heater was fabricated by connecting all sixteen heater wires in series. With this wiring arrangement, the current leads to and from the heater were in adjacent holes in the ceramic core. This resulted in large voltage gradients within the alumina core with consequent dielectric breakdown of the alumina at core temperatures around 1400 °C. The heater wiring was subsequently changed to a series-parallel arrangement in which the heater was wired as two sets of eight series-connected wires with these two sets connected in parallel. This greatly reduced the voltage gradients in the ceramic core and we had no further trouble with dielectric breakdown.

Another problem that caused some concern was that of a-c pickup at high temperatures by the core thermocouple. The physical arrangement of the apparatus made it difficult to shield this thermocouple. Probably one of the best procedures would have been to use commercially-available metal-sheathed thermocouples fabricated by swaging techniques. The temperatures involved would have required the use of thermocouples with noble-metal sheaths, thus greatly increasing the cost of the thermocouples. Since it was desired to use a new thermocouple for each specimen (the high temperatures could cause thermocouples to lose their calibration), the total cost would have been quite high. It was found possible to use unshielded thermocouples by reading the output using a electronic integrating digital voltmeter having 140 dB common-mode rejection.

5.3. Calculation Procedure

A computer program was written to enable calculation of thermal conductivity values from the data which were obtained. The input to the computer consisted of the voltmeter and ammeter readings and the thermocouple positions and emfs for each test. The calculation procedure was as follows:

1. The ammeter and voltmeter readings were adjusted slightly, if necessary, by sub-programs which contained the meter calibrations.

2. Temperatures were computed from the thermocouple emfs using sub-programs which contained the thermocouple calibrations.

3. The power output per unit length in the absence of longitudinal heat losses was computed for each position along the ceramic core using the leading term in eq. (17). The resistance per unit length, β, of the heater wire was computed using an equation representing NBS-obtained data on the temperature-dependence of Pt - 40% Rh alloy. It was assumed that the heater wire was at the temperature, T_h, measured at the center of the core.

4. The average core temperature at each longitudinal position was computed using eq. (21).

5. A fourth-order polynomial was fitted (by least-squares) to the (usually 19) values of $\bar{v}(z)$. From this equation and an equation which was used to compute C, the longitudinal thermal conductance of the core, the second term in eq. (17) was evaluated.

6. From these values of Q(z), the mean thermal conductivity, $\lambda^*(T_b, T_a)$, was computed at each position using eqs. (32) and (33). The computer program contained a value for k_s, the thermal conductivity of the brass shell, and an equation for computing k_c, the thermal conductivity of the ceramic core, as

a function of temperature. Since no knowledge was available
regarding the thermal contact resistances, R_a and R_b were
set equal to zero. A separate subprogram was used to compute
$U(z)$, the correction for longitudinal heat flow in the specimen.

7. An equation of the form $\lambda^*(25, T_a) = a + b T_a + c T_a^2 + d T_a^n$ ($n \geq 3$)
   was fitted (least-squares) to the computed $\lambda^*(T_b, T_a)$ values
   corresponding to the mid-height of the apparatus, the λ^* values
   being adjusted slightly so that they all corresponded to a
   cold side temperature of $T_b = 25$ °C.

8. The thermal conductivity was computed from this equation using
   the relation

$$\lambda(T_a) = \lambda^*(T_b, T_a) + (T_a - T_b) \frac{\partial \lambda^*(T_b, T_a)}{\partial T_a} \qquad (34)$$

   which is obtained by differentiation of eq. (5).

9. The computed λ^* values and the fitted curves for λ^* and λ were
   stored on a magnetic tape which later was used to generate the
   plots (figures 6 through 16) in the next section.

6. Results

Prior to undertaking measurements of the thermal conductivity of any of the supplied soil samples, we measured the thermal conductivity of a sample of diatomaceous earth. We had previously [1] measured the thermal conductivity of this same lot of diatomaceous earth in an apparatus in which both the hot and the cold sides of the specimen were heated so that λ could be measured directly rather than being computed from λ^*. Further, in this earlier apparatus the ends were heated so that there was no need to make corrections for longitudinal heat flow in the core or in the specimen. Measurement of this lot of diatomaceous earth in the present apparatus provided a check on the corrections for longitudinal heat flow (which were rather large because of the low thermal conductivity of diatomaceous earth) and also provided a check on the procedure used to compute λ from the measured λ^* values.

The solid triangles shown in figure 6 represent the $\lambda^*(25, T_a)$ data points obtained in the present apparatus plotted versus T_a, the hot side temperature. The solid curve is the cubic of least-squares fit to these data. The dashed curve represents the $\lambda(T_a)$-values computed using eq. (34). The open circles represent the smoothed thermal conductivity values obtained earlier by Flynn[1] on diatomaceous earth from the same lot as was used in the present measurements. The agreement is seen to be good.

Figures 7 through 16 show the measured λ^*-values, the least-squares λ^*-curves, and the derived λ-curves for each of the nine soil samples supplied by Sandia. The data correspond to monotonic heating to the maximum temperatures shown. Measurements have been completed on two samples, designated by solid triangles and open squares, at nominally the same density, for calcareous soil, dune sane, and coastal plains clay. At the request of Sandia, the second run on Ottawa sand was made with a lower density than was used for the first specimen.

Figure 17 shows λ^* for all of the specimens measured to date while figures 18 and 19 illustrate the corresponding values of λ. Note that each set of curves tends to converge to a common region at high temperatures. The key to these curves is given below.

Symbol	Specimen	Average Density kg m^{-3}
DE	diatomaceous earth	150
C	calcareous	2000
GD	granitic detrital	1920
DS	dune sand	1570
M	magnesian	1760
P	podzol	1760
CP	coastal plains	1335
L	laterite	1490
EP	estancia playa	1540
OS_1	Ottawa sand	1760
OS_2	Ottawa sand	1570
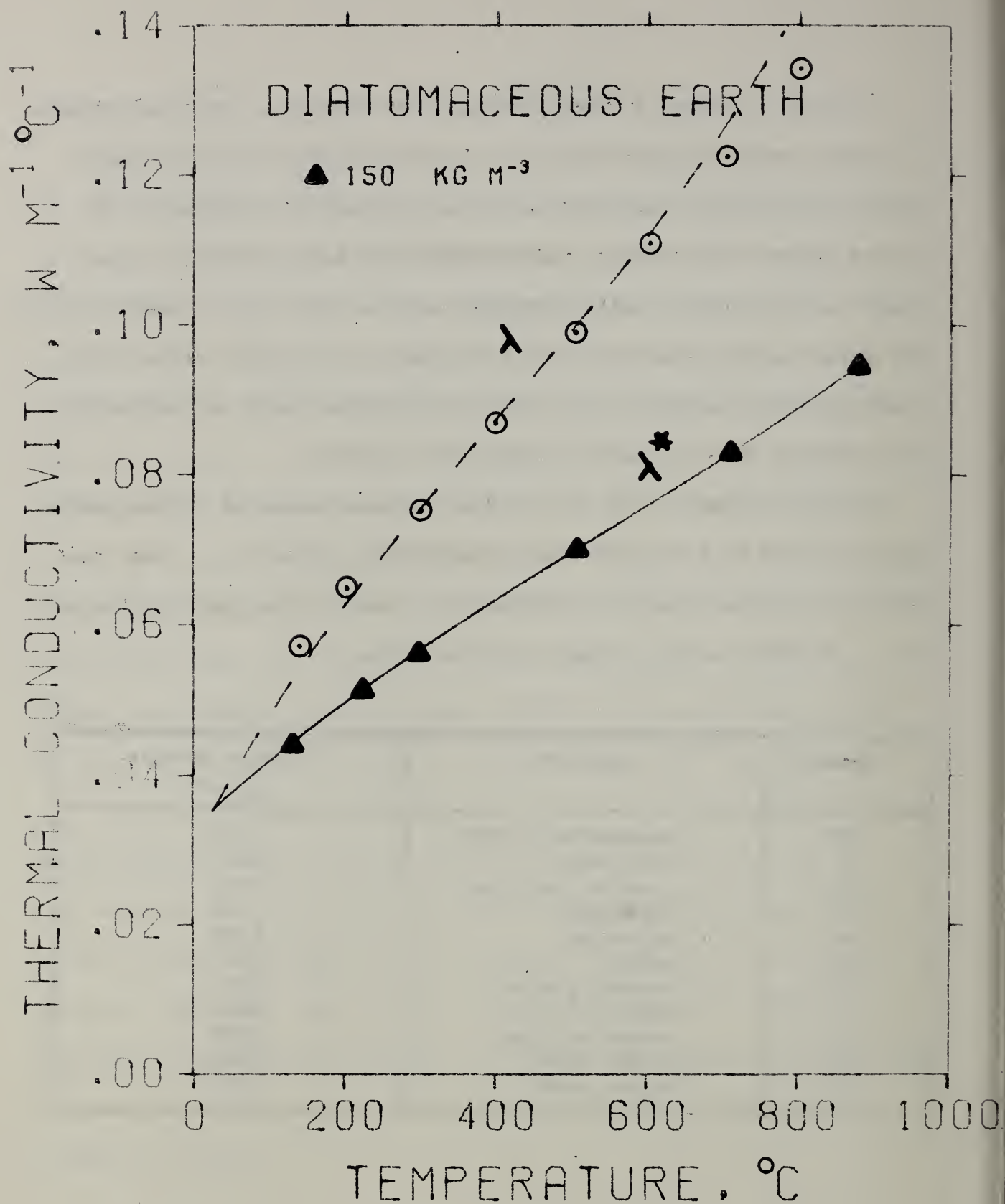
Figure 6.   Thermal conductivity of diatomaceous earth at a density of
0.15 x 10³ kg m⁻³.   The solid curve represents an equation of
the form $\lambda^{*}(25,T_a) = a + bT_a + cT_a^{2} + dT_a^{3}$.   The open circles
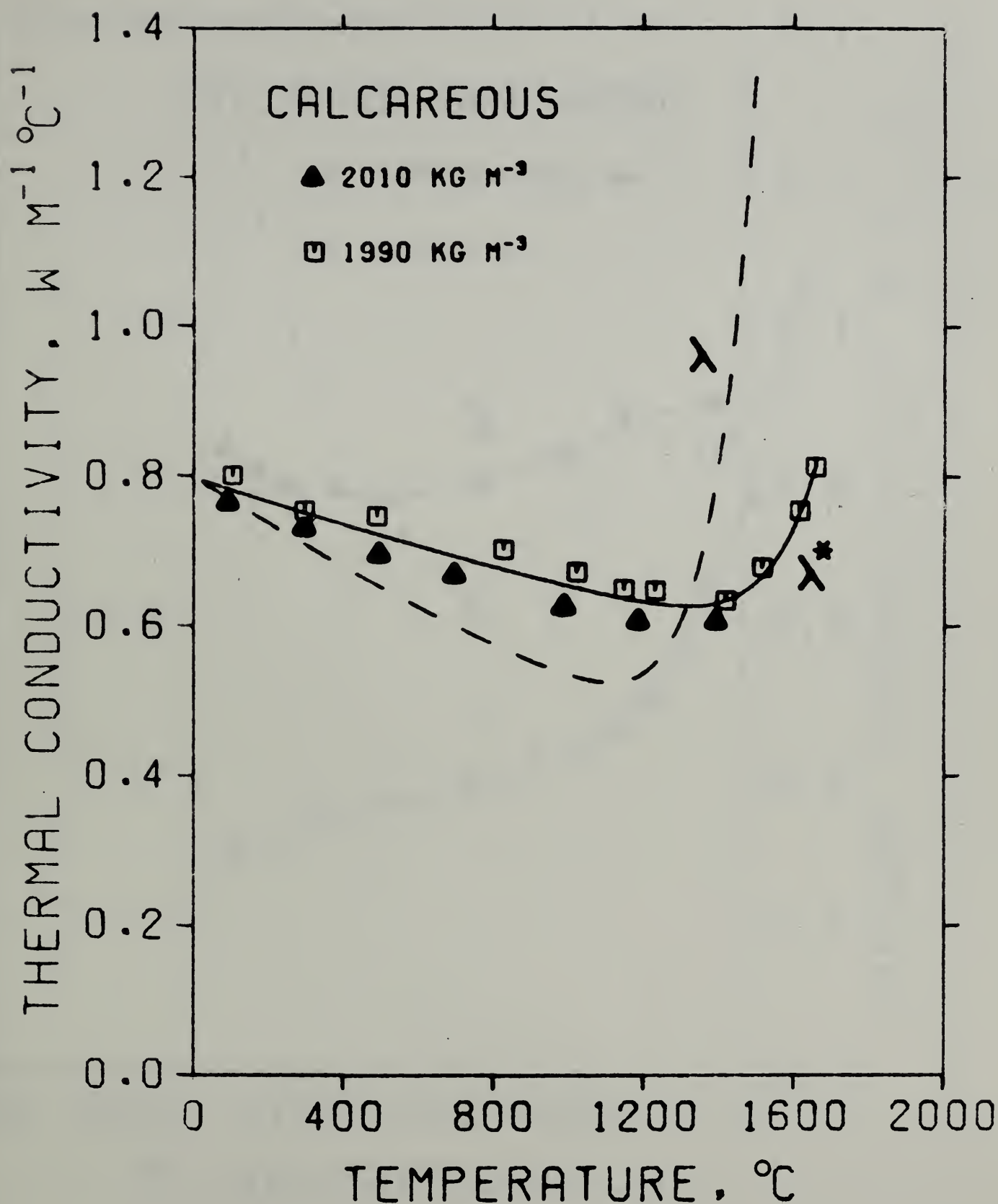represent the smoothed values obtained earlier by Flynn[1].

36

Figure 7. Thermal conductivity of calcareous soil at densities of 2.01 x 10³ and 1.99 x 10³ kg m⁻³. The solid curve represents an equation of the form $\lambda^*(25,T_a) = a + bT_a + cT_a^2 + dT_a^{19}$.
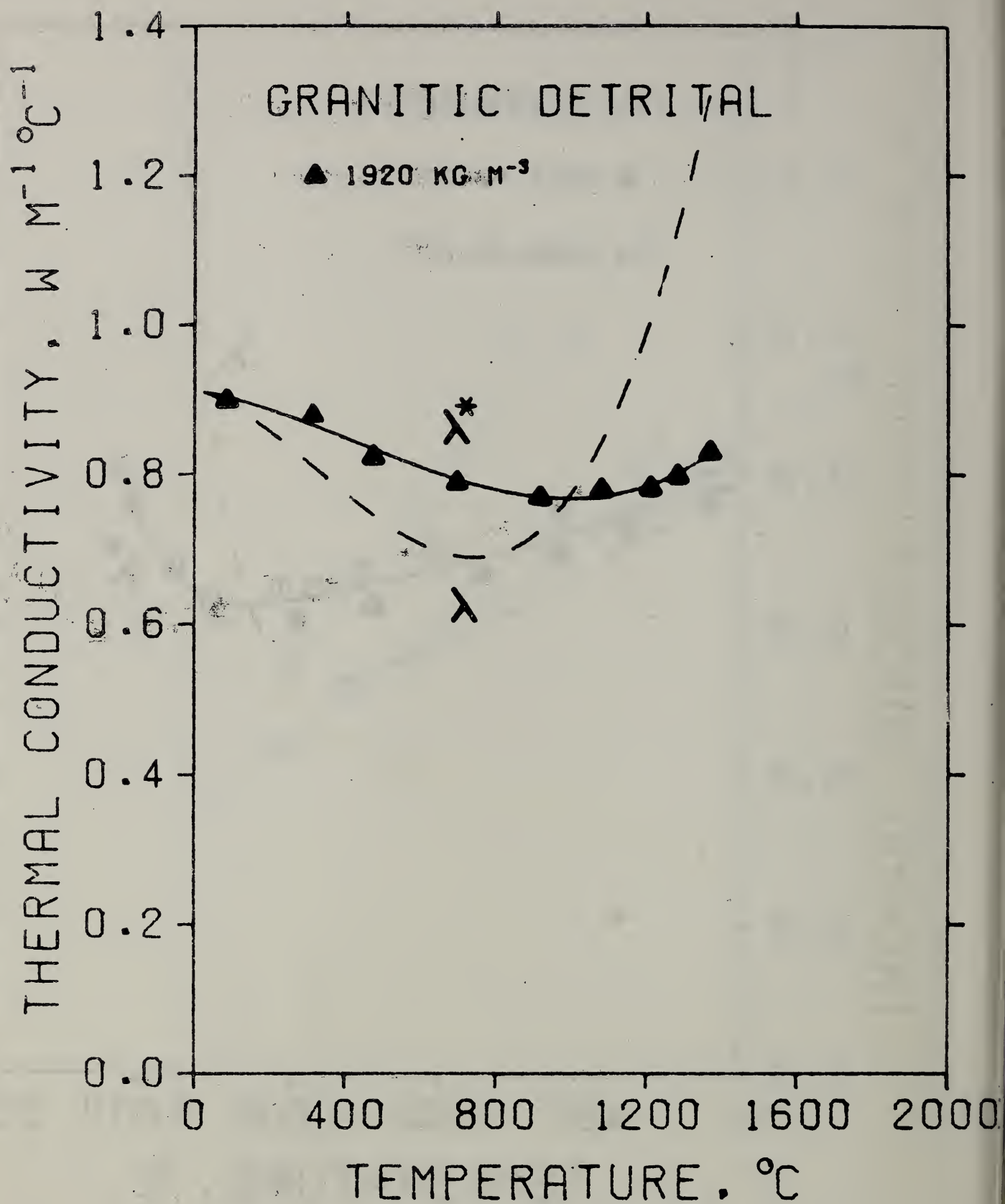
Figure 8. Thermal conductivity of granitic detrital soil at a density of 1.92×10^3 kg m^{-3}. The solid curve represents an equation of the form $\lambda^*(25,T_a) = a + bT_a + cT_a^2 + dT_a^3$.
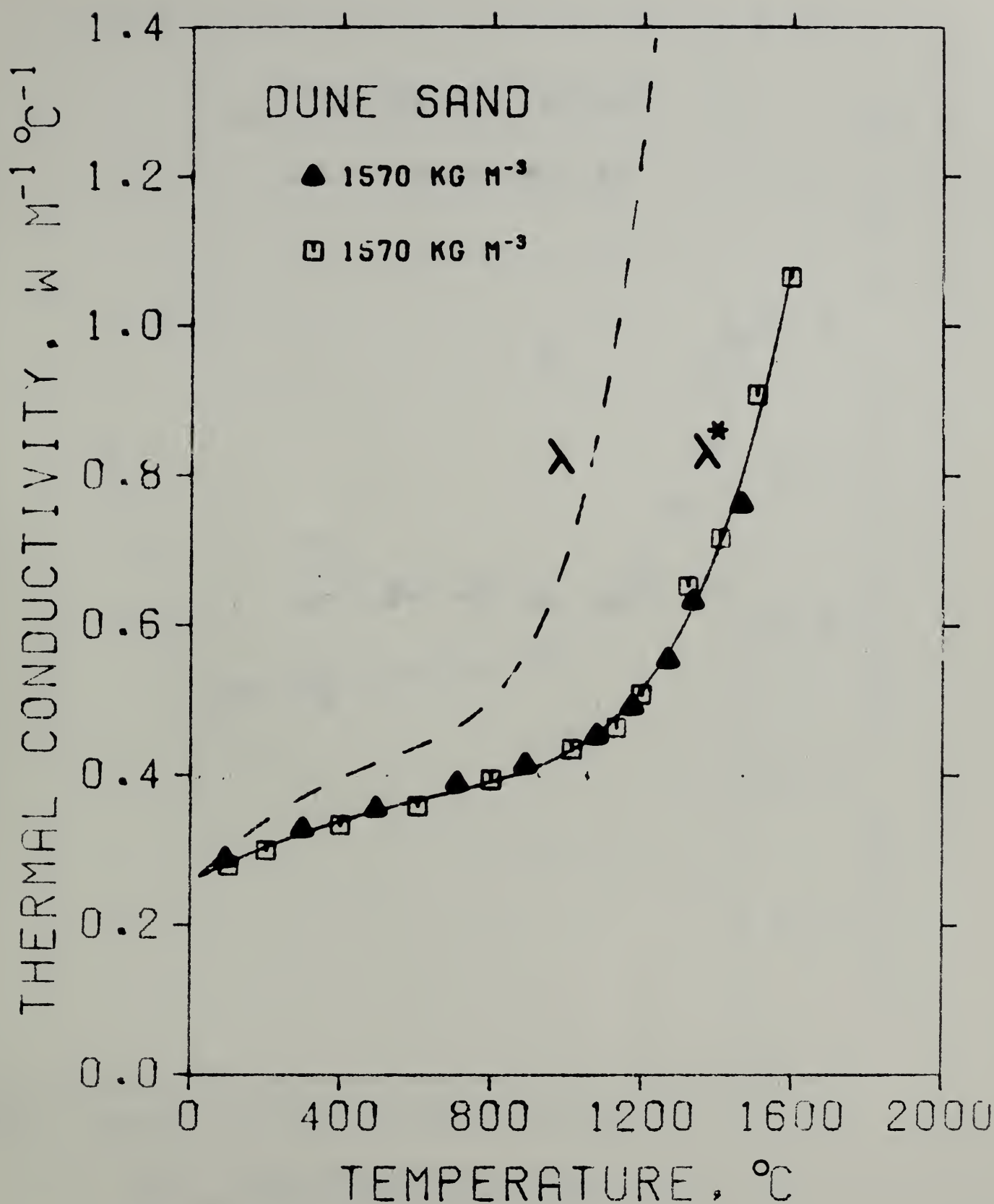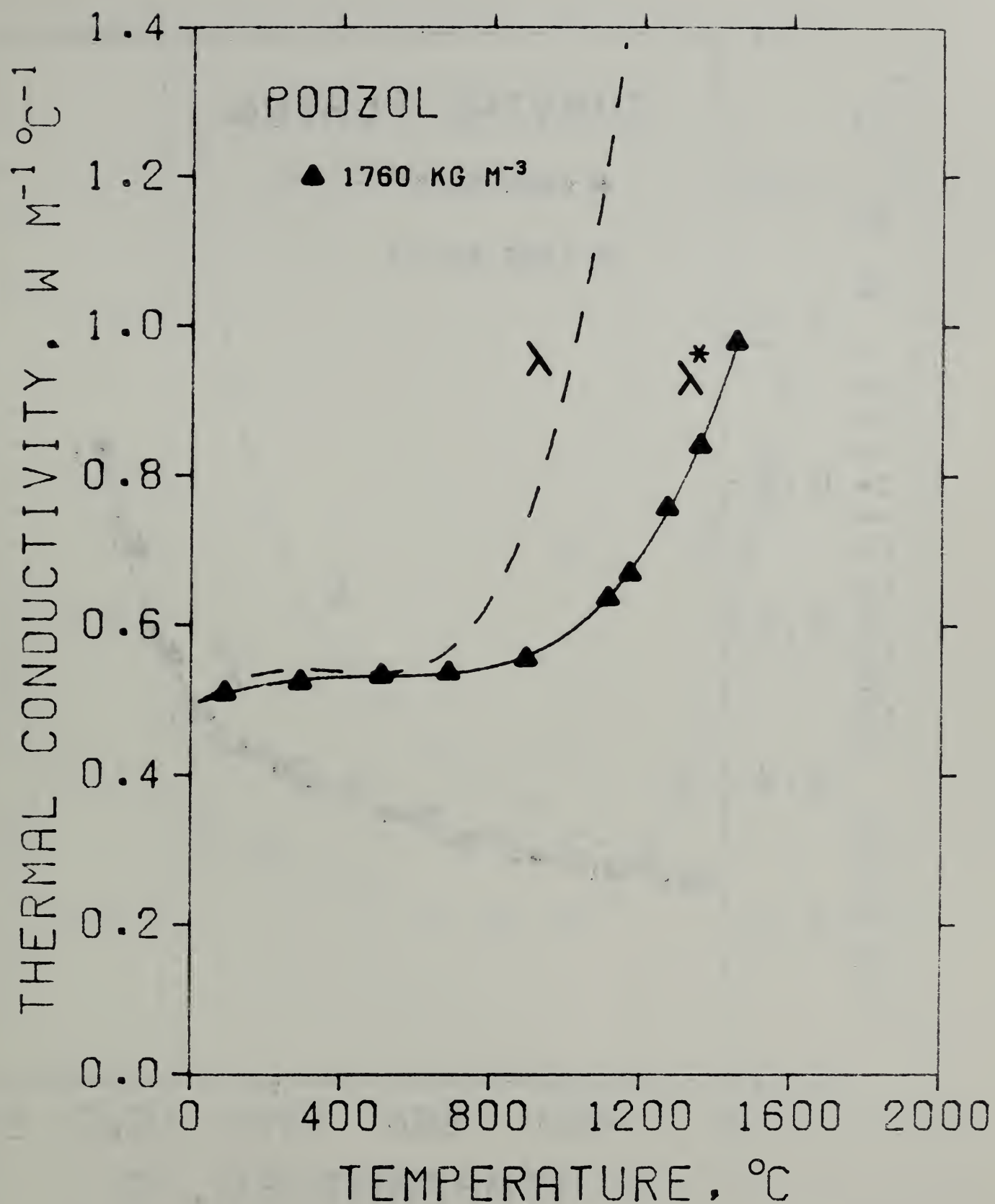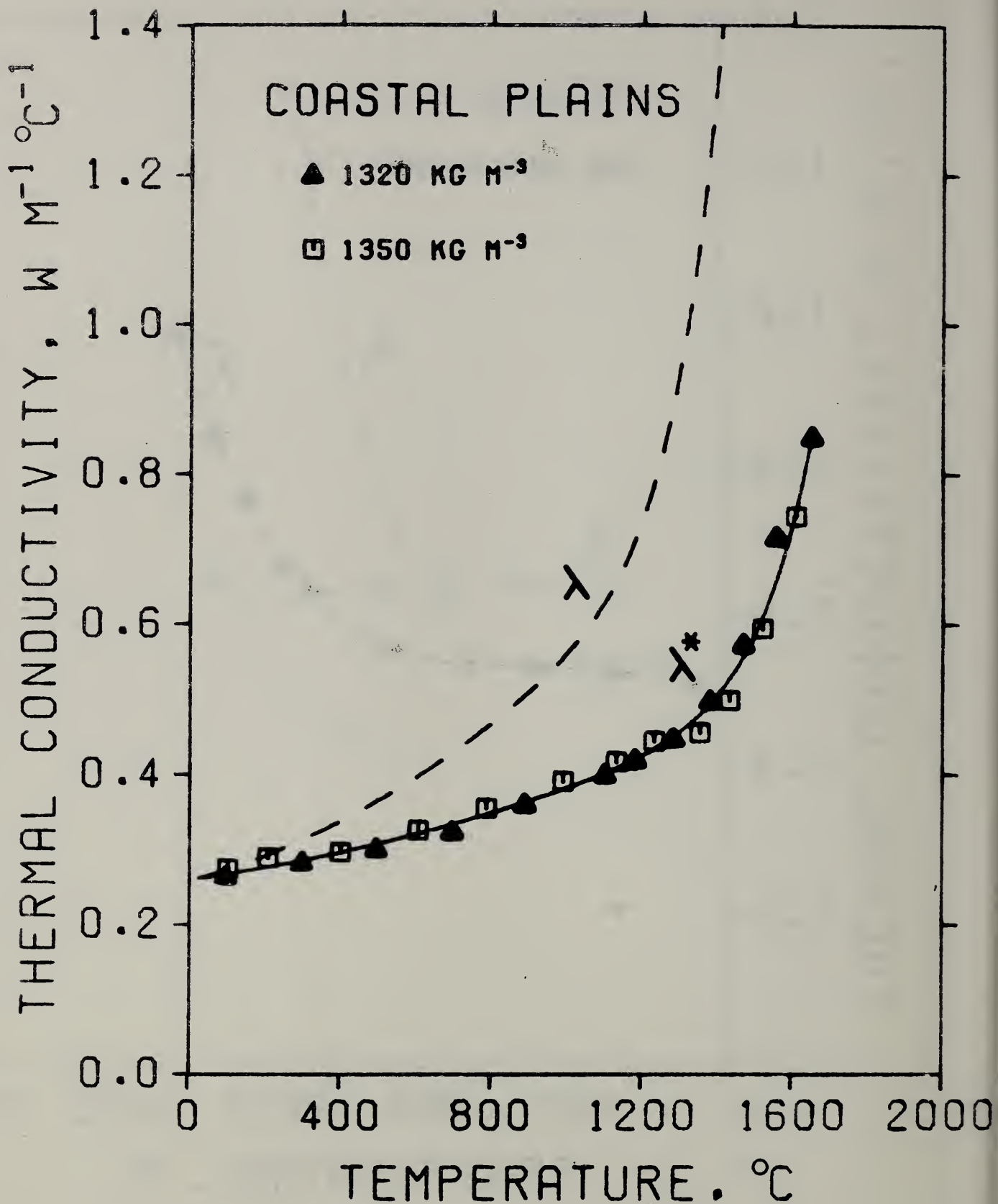
Figure 9. Thermal conductivity of two specimens of dune sand, each at a density of 1.57×10^3 kg m^{-3}. The solid curve represents an equation of the form $\lambda^*(25,T_a) = a + bT_a + cT_a^2 + dT_a^6$.
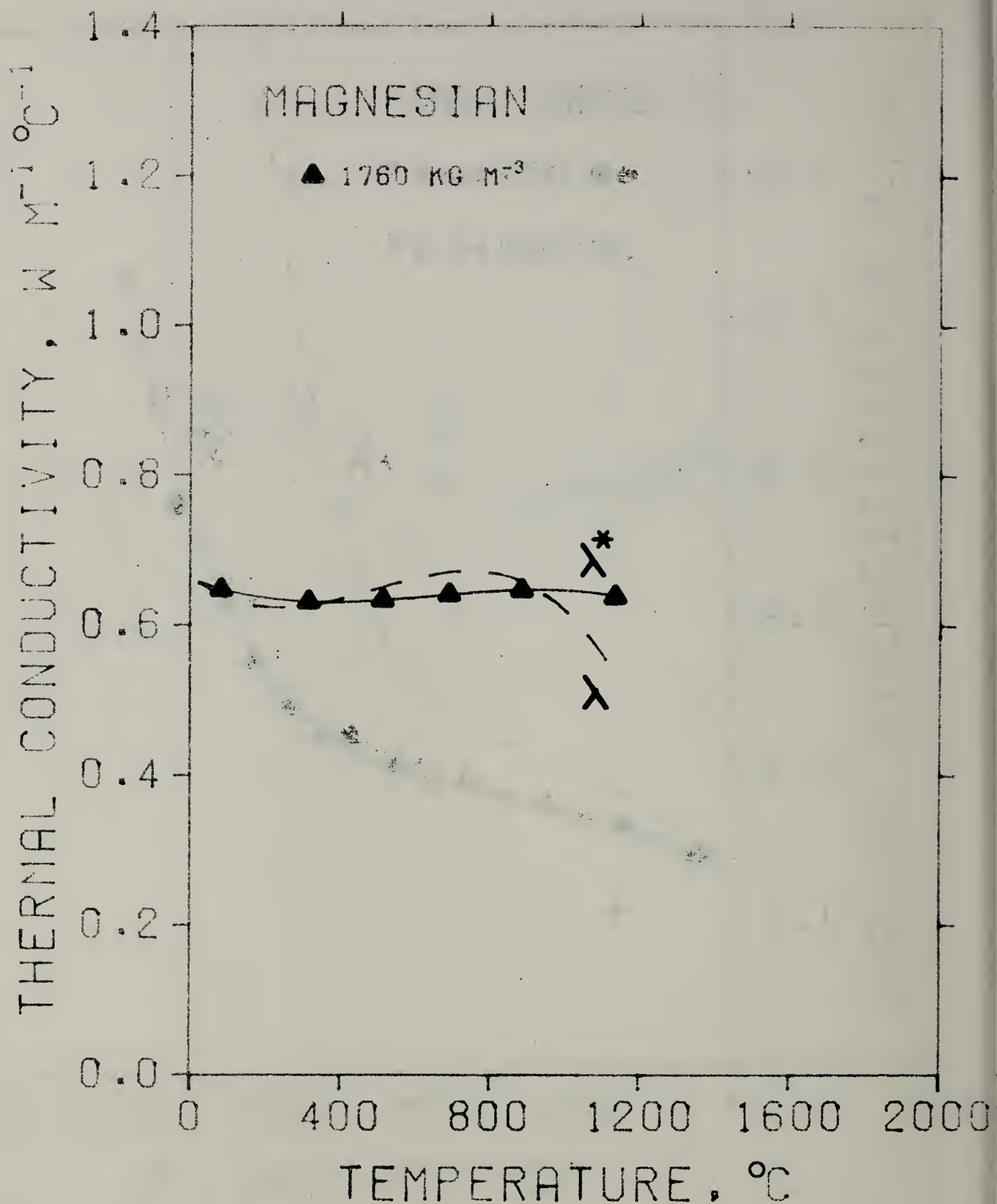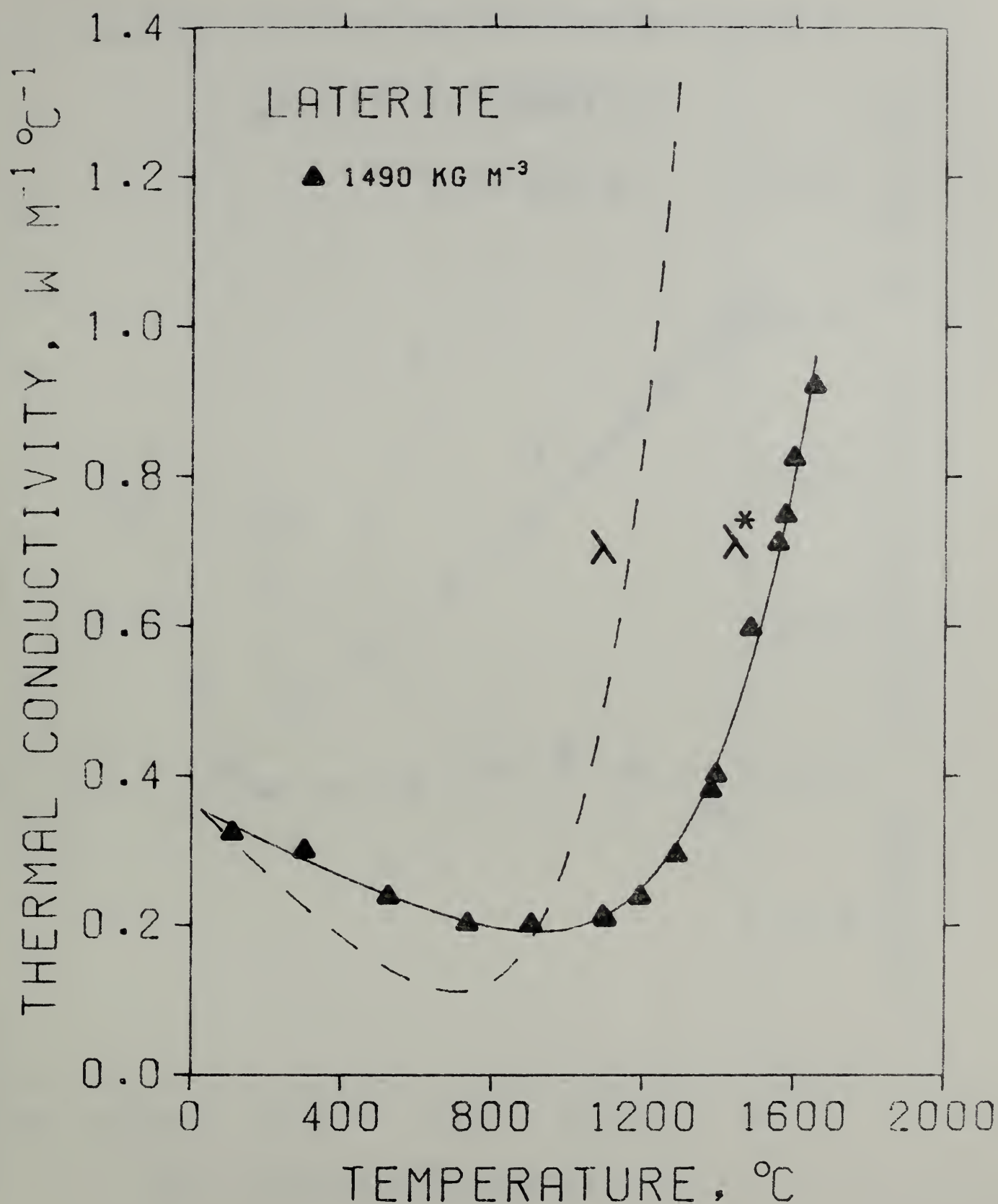
Figure 10. Thermal conductivity of magnesian soil at a density of
1.76×10^3 kg m^{-3}. The solid curve represents an equation
of the form $\lambda^*(25, T_a) = a + bT_a + cT_a^2 + dT_a^3$.

Figure 11. Thermal conductivity of podzol soil at a density of 1.76×10^3 kg m^{-3}. The solid curve represents an equation of the form $\lambda^*(25,T_a) = a + bT_a + cT_a^2 + dT_a^4$.

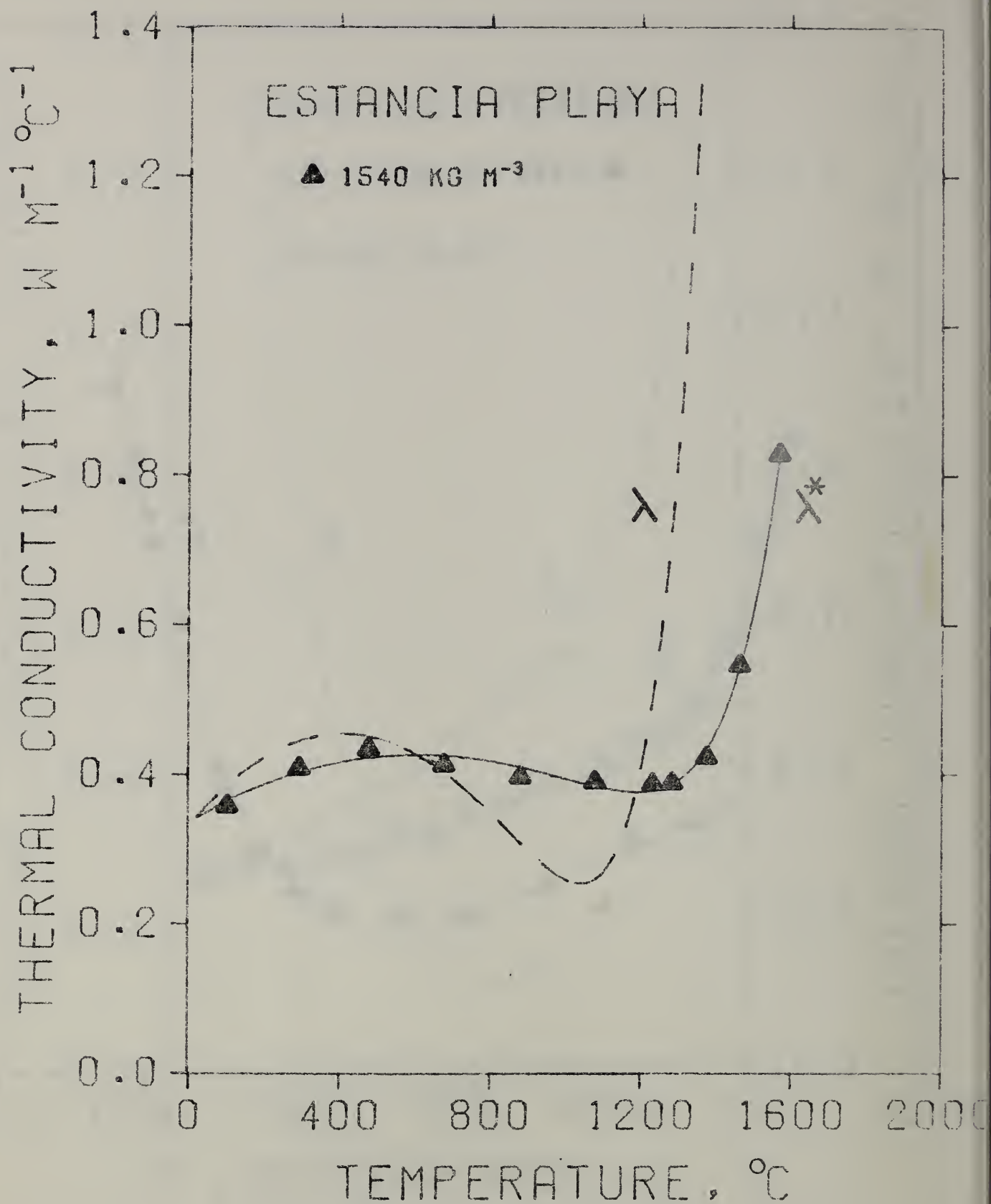Figure 12. Thermal conductivity of coastal plains clay at densities of 1.32 x 10³ and 1.35 x 10³ kg m⁻³. The solid curve represents an equation of the form $\lambda^*(25, T_a) = a + bT_a + cT_a^2 + dT_a^{12}$.

Figure 13. Thermal conductivity of laterite soil at a density of 1.49×10^3 kg m^{-3}. The solid curve represents an equation of the form $\lambda^*(25, T_a) = a + bT_a + cT_a^2 + dT_a^6$.
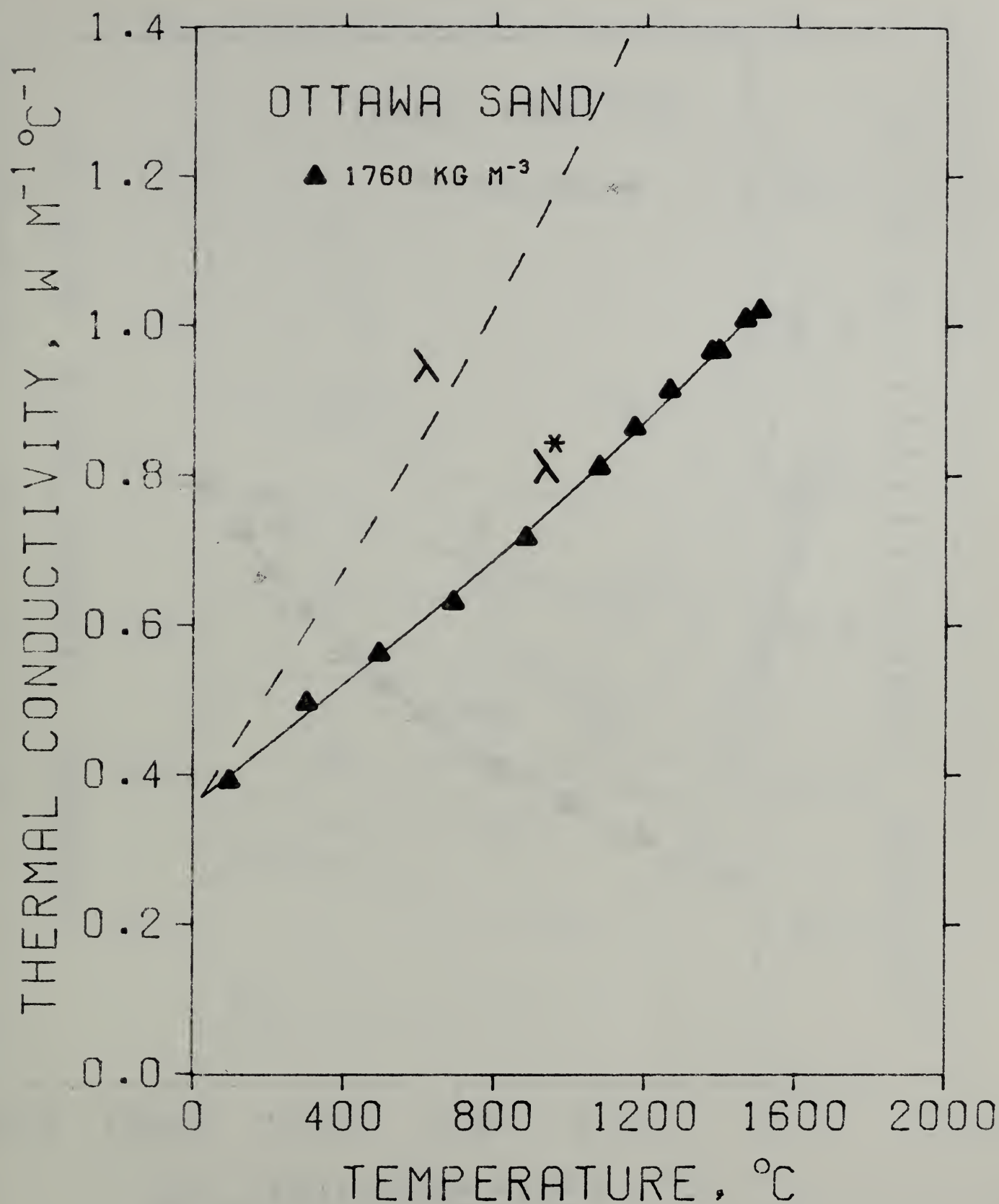
43

Figure 14. Thermal conductivity of estancia playa soil at a density of 1.54 x 10³ kg m⁻³. The solid curve represents an equation of the form $\lambda^*(25,T_a) = a + bT_a + cT_a^2 + dT_a^{11}$.

44

Figure 15. Thermal conductivity of Ottawa sand at a bulk density of 1.76 x 10³ kg m⁻³. The solid curve represents an equation of the form $\lambda^*(25,T_a) = a + bT_a + cT_a^2 + dT_a^3$.

45
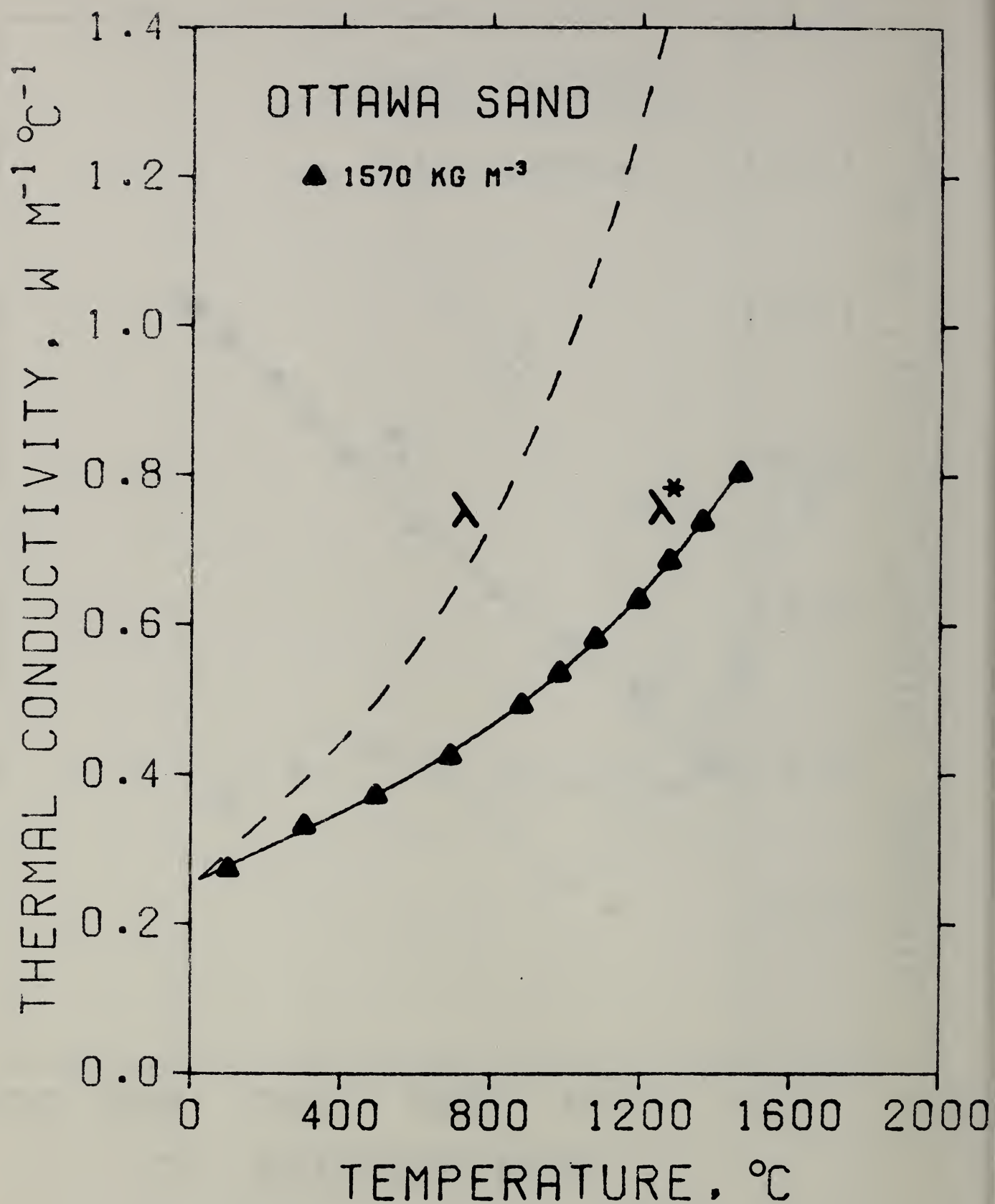
Figure 16. Thermal conductivity of Ottawa sand at a bulk density of
1.57 x 10^3 kg m^{-3}. The solid curve represents an equation
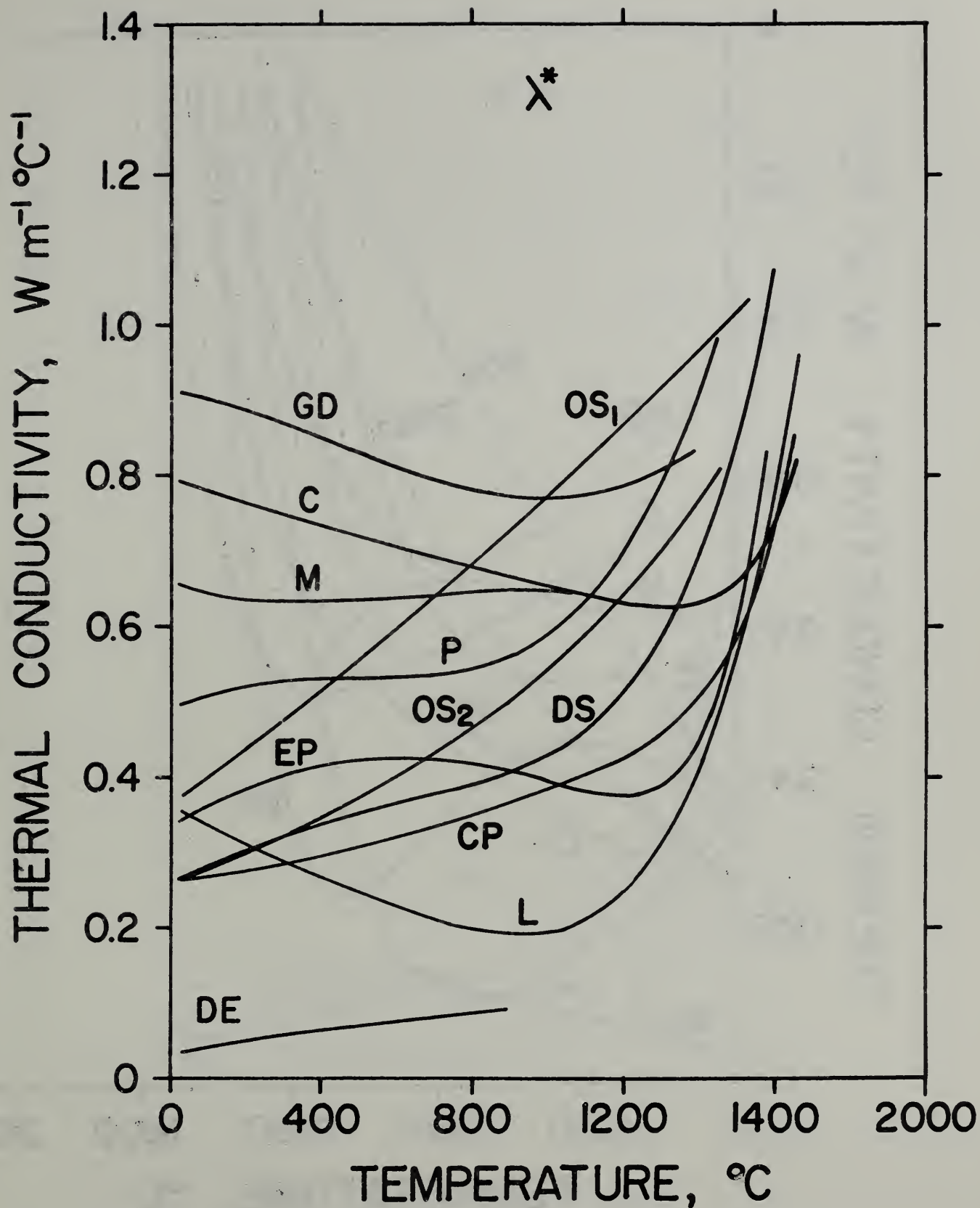of the form $\lambda^*(25,T_a) = a + bT_a + cT_a{}^2 + dT_a{}^3$.

46

Figure 17. The effective thermal conductivity, $\lambda^*(25, T_a)$, of all of the specimens measured to date plotted versus the hot-side temperatures.
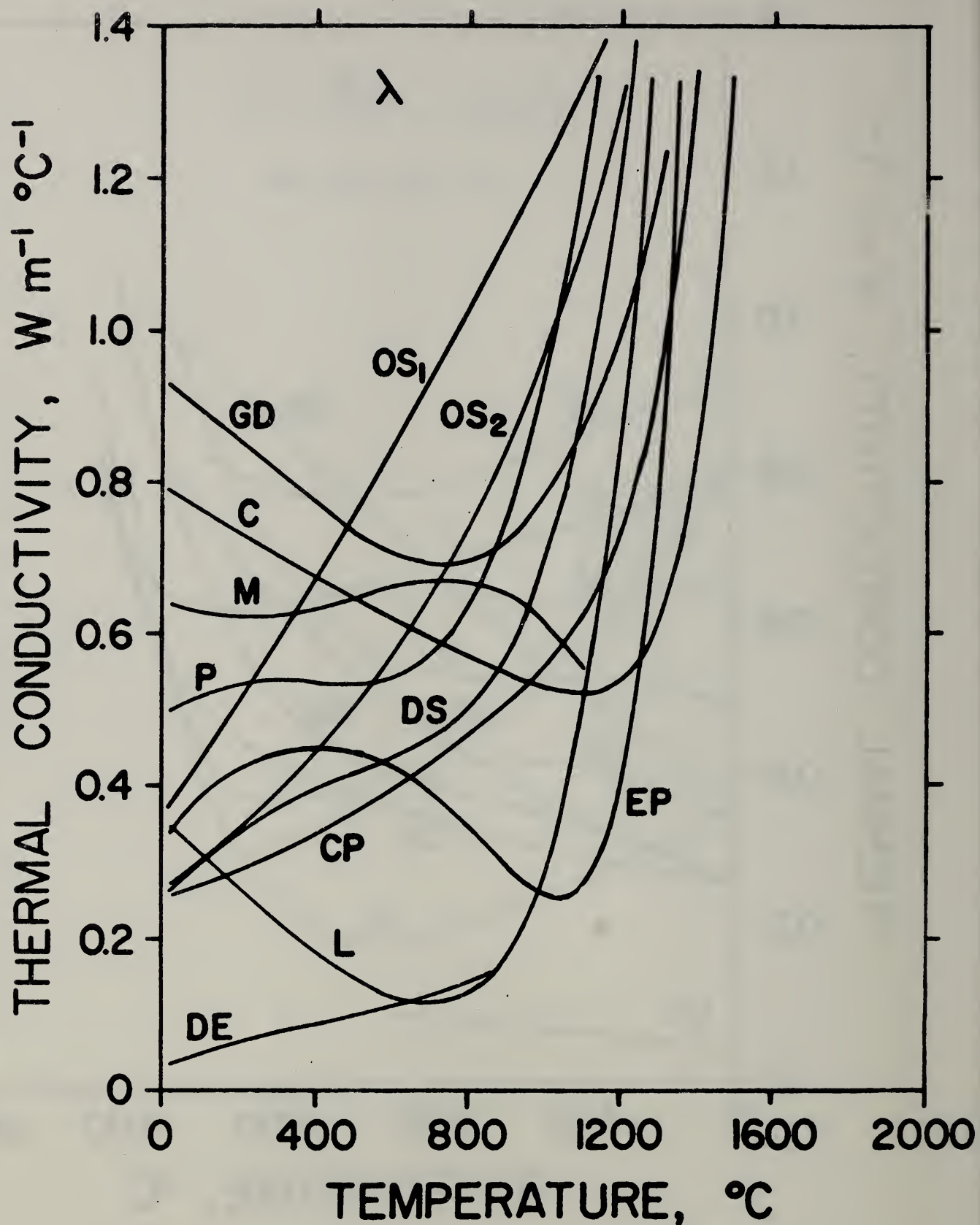
Figure 18. The derived thermal conductivity, $\lambda(T_a)$, of all of the specimens measured to date plotted versus temperature. The curves are truncated near $\lambda = 1.4$ W m^{-1} °C^{-1}.
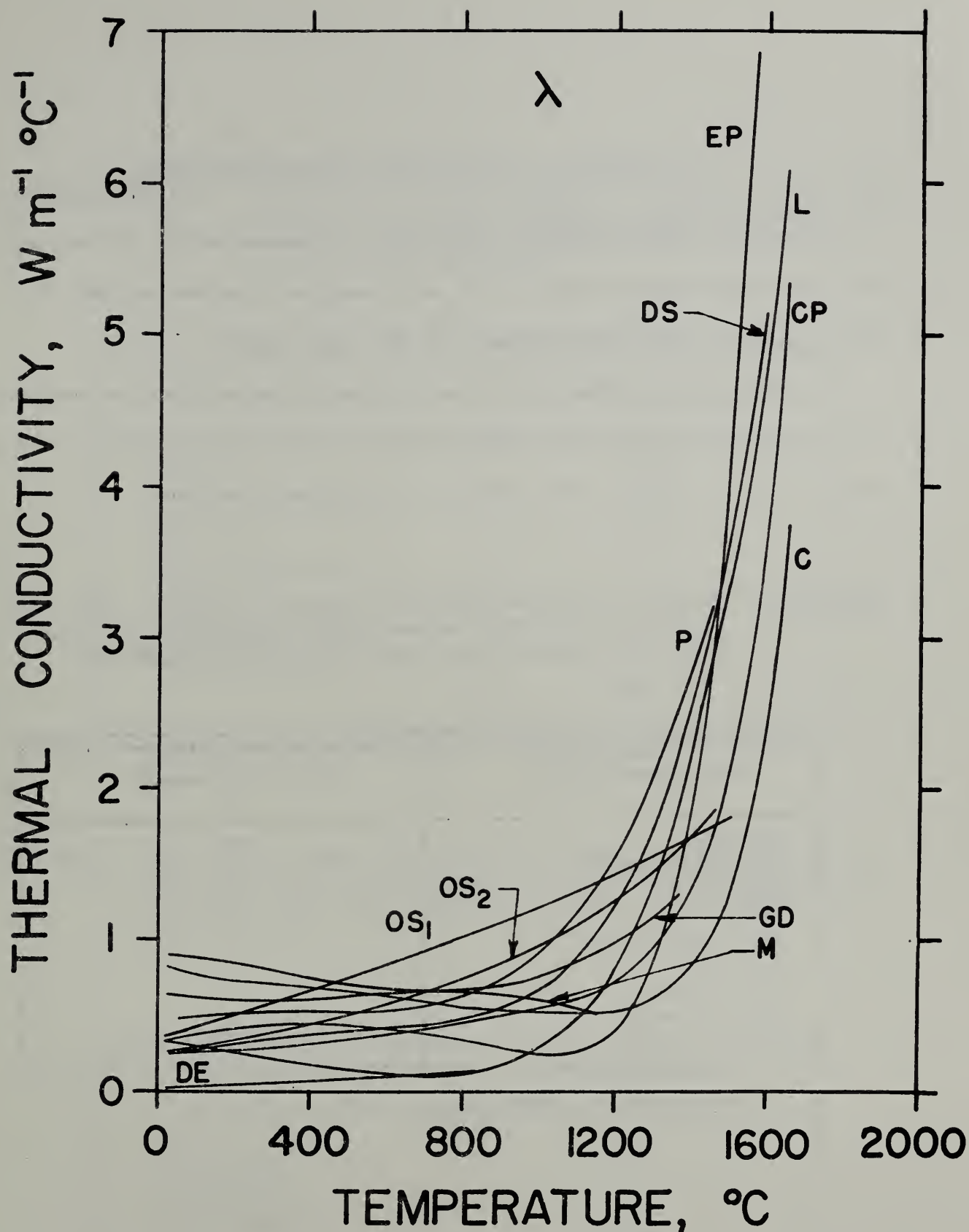
48

Figure 19. The derived thermal conductivity, $\lambda(T_a)$, of all the specimens measured to date plotted versus temperature. The vertical scale has been changed to enable showing the high-temperature behavior.

49

7. Appendix A: Soil Sample Characterization

A private testing laboratory carried out measurements of the particle size distribution of all of the soil samples supplied to NBS. We hope to include these measurements in the final report.

The University of New Mexico carried out X-ray diffraction analyses of the soil samples and then made estimates of the composition and melting range of each soil[5]. These results are presented below:

CALCAREOUS   Common to arid and semi-arid regions of world. CaO, one of 12 most plentiful oxides of the earth's crust, tends to have very high melting range and will cause gassing.

Soil Constituents	Estimated Amount %
Calcite	75
Montmorillonite	8
Quartz	8
Dolomite	3
Muscovite-illite	2
Goethite	1
Oligoclase	1
Trace Minerals	2
	100

Estimated Soil-Melt Range: 1950 to 2050 °C

GRANITIC DETRITAL   These soils with a high-alkali feldspar content have
                     a low-melting range. They are typical of many
                     detrital soils, which comprise about a quarter of
                     total land area of world.

Soil Constituents	Estimated Amount %
Quartz	45
Albite	20
Microcline	10
Calcite	6
Montmorillonite	7
Illite-mica	3
Chlorite	3
Mixed-layer clays	4
Trace Minerals	2
	100

Estimated Soil-Melt Range: 1200 to 1320 °C

DUNE SAND   Typical of barchan sand dunes of world, representative of
             about 7% of total land area of world. Consists largely of
             siliceous sand, SiO_2, comprising nearly 60% of oxides of
             earth's crust.

Soil Constituents	Estimated Amount %
Quartz	60
Oligoclase	25
Microcline	10
Clinopyroxene	5
	100

Estimated Soil-Melt Range: 1300 to 1450 °C

MAGNESIAN   Representative of soils derived from gabbros, basalts, and
              dolomites. MgO is one of the 12 most plentiful oxides of
              the earth's crust.

Soil Constituents	Estimated Amount %
Talc	35
Penninite	30
Oligoclase	25
Calcite	5
Trace minerals	5
	100

Estimated Soil-Melt Range: 1350 to 1435 °C

PODZOL   Leached organic soils of woodland regions of temperate zones
           of world, which comprise about a quarter of total land area
           of world.

Soil Constituents	Estimated Amount %
Quartz	60
Microcline	15
Albite	10
Chlorite	5
Hornblende	5
Trace Minerals	5
	100

Estimated Soil-Melt Range: 1350 to 1450 °C

52

COASTAL PLAINS CLAY   Typical of well-weathered soils, representative of
                       about 15% of total land area of world. Soil may
                       seal and build gas pressure when saturated.

Soil Constituents	Estimated Amount %
Quartz	45
Kaolinite	25
Montmorillonite	25
Trace minerals	5
	100

Estimated Soil-Melt Range: 1600 to 1620 °C

LATERITE   Representative of tropical humid regions of world, comprising
            more than 10% of total land area of world. FeO and Fe_2O_3
            are two of most plentiful oxides of the earth's crust.

Soil Constituents	Estimated Amount %
Goethite	55
Gibbsite	30
Magnetite	5
Maghemite	5
Ilmenite	5
	100

Estimated Soil-Melt Range: 1900 to 1950 °C

ESTANCIA PLAYA   Typical of very saline bolson playas of the world; most
extreme chemical corrosive action upon heating.

Soil Constituents	Estimated Amount %
Gypsum	31.5
Calcite	13.0
Dolomite	24.5
Quartz	7.5
Feldspar	5.0
Halite	7.5
Clays	5.0
Trace minerals	6.0
	100.0

Estimated Soil-Melt Range: 1350 to 1400 °C

OTTAWA SAND   Commercially available material that might possibly be used
as a standard in comparing results from different laboratories.

Essentially pure quartz

Estimated Melting Point: 1720 °C

8.   Appendix B: Results of Differential Thermal Analyses of Soil Samples

The soil samples were ground to pass through a 100-mesh sieve.
After drying each sample at 140 °C for two hours, the analyses were per-
formed using an R. L. Stone #230 differential thermal analysis (DTA)
instrument. Each sample was placed in   a platinum cup and tapped
lightly to fill possible air spaces. The aluminum oxide powder used as
a reference material was placed in a similar cup. The sample and refer-
ence cups were installed within a platinum enclosure in the furnace
chamber. The temperature difference between the sample and reference
cups was monitored by a differential thermocouple with a junction in
each cup. The enclosure temperature was monitored by a thermocouple
having its hot junction located between the sample and reference cups.

For each soil sample, DTA curves were obtained at heating rates of
10, 20, and 30 °C/minute with helium flowing through the sample enclo-
sure; on certain samples, cooling curves at one or more rates were also
obtained. Heating curves at 30 °C/minute with dry air flowing through
the sample enclosure were also obtained for each sample. No significant
differences were apparent between the DTA curves in helium and in air.

The following table summarizes the DTA results obtained on heating.
The characteristic temperatures A, B, and D were determined as shown in
figure 20.

In addition to carrying out differential thermal analyses (DTA) on each sample to about 1400 °C, thermogravimetric analyses (TGA) were made on each sample to 500 °C or higher in order to determine the amount of free or bound water coming out of the sample. The TGA measurements were made on undried samples in air at a heating rate of 15 °C/minute.

Representative results of the DTA and TGA tests are shown in figures 21 through 38.
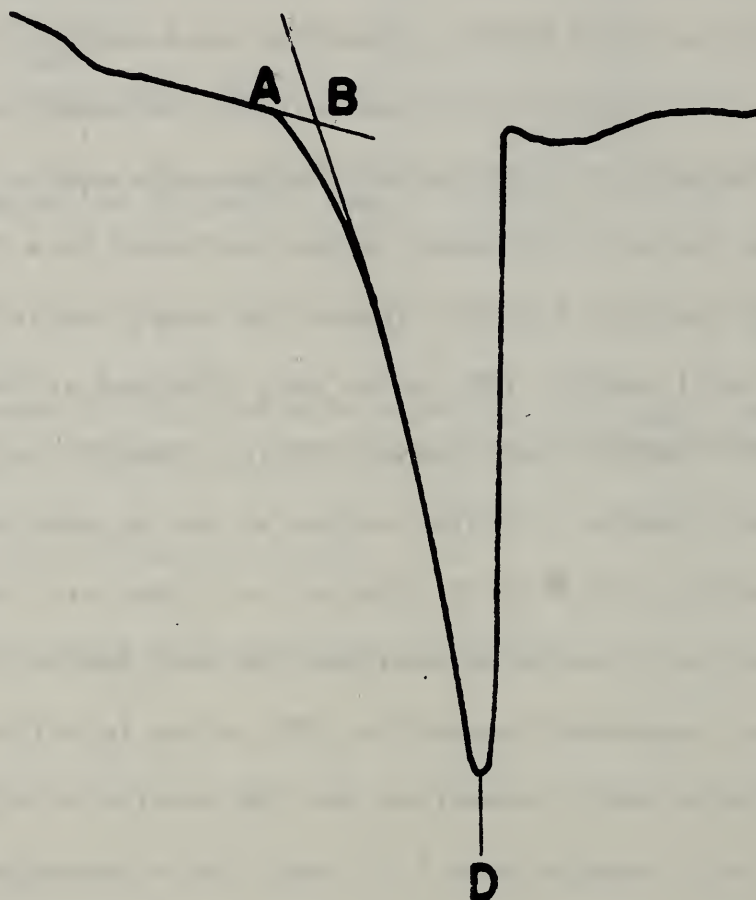

Figure 20. Scheme utilized to determine the temperatures A, B, and D which characterize a particular endotherm or exotherm. The ordinate represents the temperature difference between the sample and reference cups; the abscissa represents the temperature of the sample enclosure.

Differential Thermal Analysis Results from Heating Curves

Material	Run	Atmosphere	Heating Rate °C/min.	Endotherm			Exotherm
				A °C	B °C	D °C	D °C
Calcareous	1	Helium	20	639	729	826	1268
	2	Helium	10	---	---	(372)	----
	3	Helium	10	704	715	782	----
	4	Helium	30	656	683	784	1265
	5	Helium	30	---	---	886	----
	6	Air	30	683	774	891	1262
Granitic Detrital	1	Helium	20	563	563	564	892
				683	683	738	---
				---	---	1156	---
	2	Helium	10	560	560	563	---
				---	---	720	---
	3	Helium	30	561	561	568	904
				725	725	782	---
				1119	1119	1160	---
	4	Air	30	562	562	570	---
				724	724	784	900
				1107	1107	1154	---
Dune Sand	1	Helium	20	---	---	224	---
				560	560	565	---
				---	---	694	---
	2	Helium	10	---	---	300	---
				561	561	567	---
	3	Helium	30	558	558	567	---
				639	660	766	---
	4	Air	30	567	567	571	---
				635	675	767	---
Magnesian	1	Helium	20	---	---	293	---
				---	---	563	---
				---	---	723	---
				---	---	791	---
	2	Helium	10	---	---	325	---
				---	---	581	---
				---	---	701	---
				---	---	716	---
	3	Helium	30	---	---	228	---
				397	526	589	---
				671	703	766	---
				---	---	1214	---
	4	Air	30	---	---	154	---
				---	---	241	---
				---	---	593	---
				671	698	770	---
				---	----	1208	---

Podzol	1	Helium	10	558	558	559	---
	2	Helium	20	570	570	576	---
	3	Helium	30	---	---	565	---
				1009	1009	1009	---
	4	Air	30	563	563	574	---
Coastal Plains	1	Helium	20	467	467	515	915
				---	---	571	---
	2	Helium	10	(270)	(331)	508	---
				---	---	567	---
	3	Helium	10	---	---	514	---
				---	---	561	---
				---	---	771	---
				---	---	950	---
	4	Helium	30	(353)	(438)	537	914
	5	Air	30	---	438	539	914
Laterite	1	Helium	20	269	286	326	---
	2	Helium	10	263	287	323	---
	3	Helium	20	---	---	328	---
	4	Helium	30	276	287	334	---
	5	Air	30	300	313	348	---
Estancia Playa	1	Helium	10	---	---	111	---
				---	---	197	---
	2	Helium	20	---	---	121	---
				---	---	567	---
				---	---	672	---
				---	---	719	---
				---	---	1222	---
				---	---	1345	---
	3	Helium	20	---	---	154	---
				---	---	570	---
				---	---	676	---
				---	---	715	---
	4	Helium	30	---	---	129	---
				---	---	589	---
				---	---	648	---
				---	---	748	---
				---	---	1231	---
				---	---	1337	---
	5	Helium	10	---	---	111	---
				---	---	340	---
				---	---	556	---
				---	---	702	---
				---	---	887	---
				---	---	950	---
	6	Air	30	---	---	607	---
				---	---	658	---
				---	---	697	---
				---	---	766	---

Ottawa Sand	1	Helium	10	---	---	182	---
				559	559	559	---
	2	Helium	20	---	---	226	---
				562	562	562	---
	3	Helium	20	---	---	221	---
				567	567	567	---
	4	Helium	30	439	558	564	---
	5	Air	30	366	561	569	---
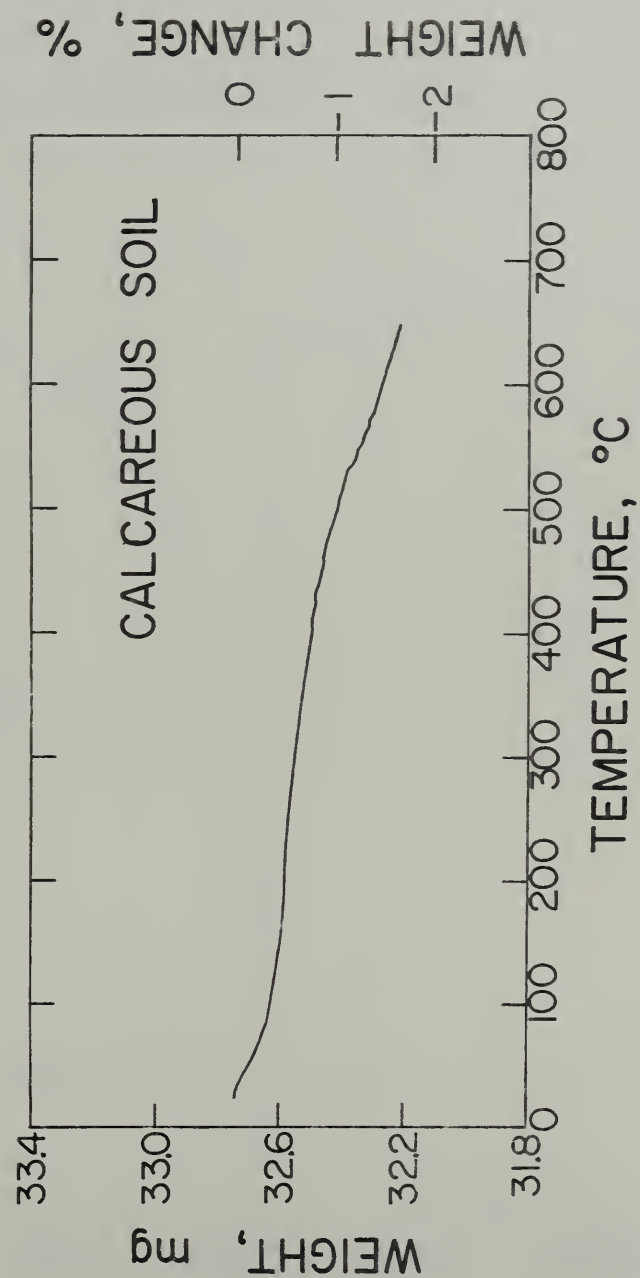
Figure 21. Thermogravimetric analysis of calcareous soil.
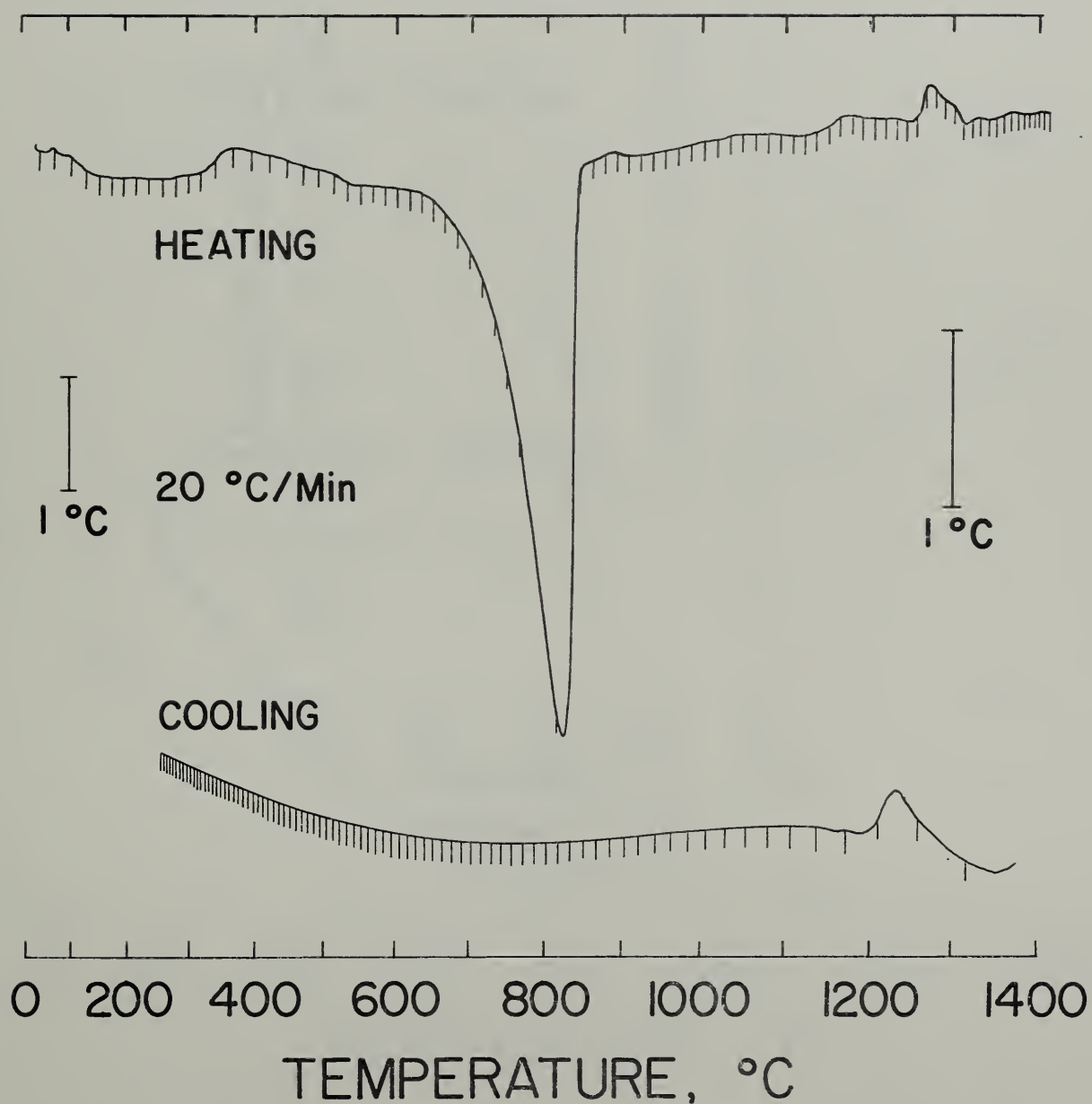
Figure 22. Differential thermal analyses of calcareous soil.
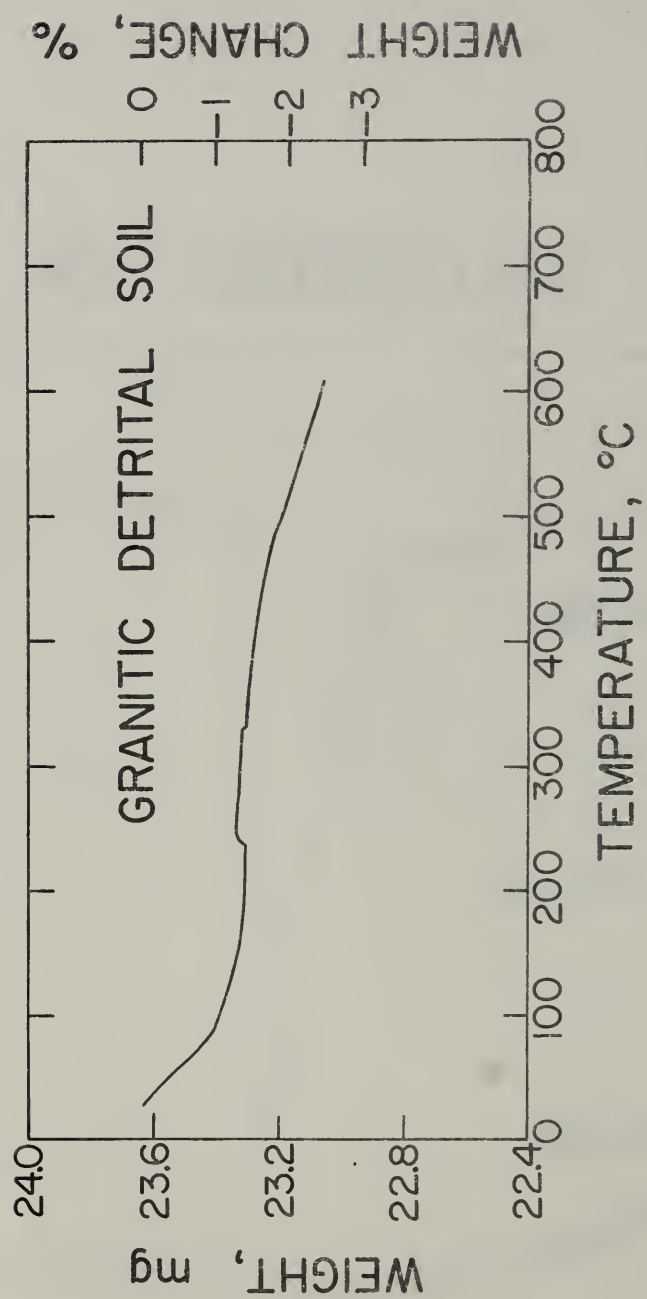
Figure 23 Thermogravimetric analysis of granitic detrital soil.

GRANITIC DETRITAL SOIL
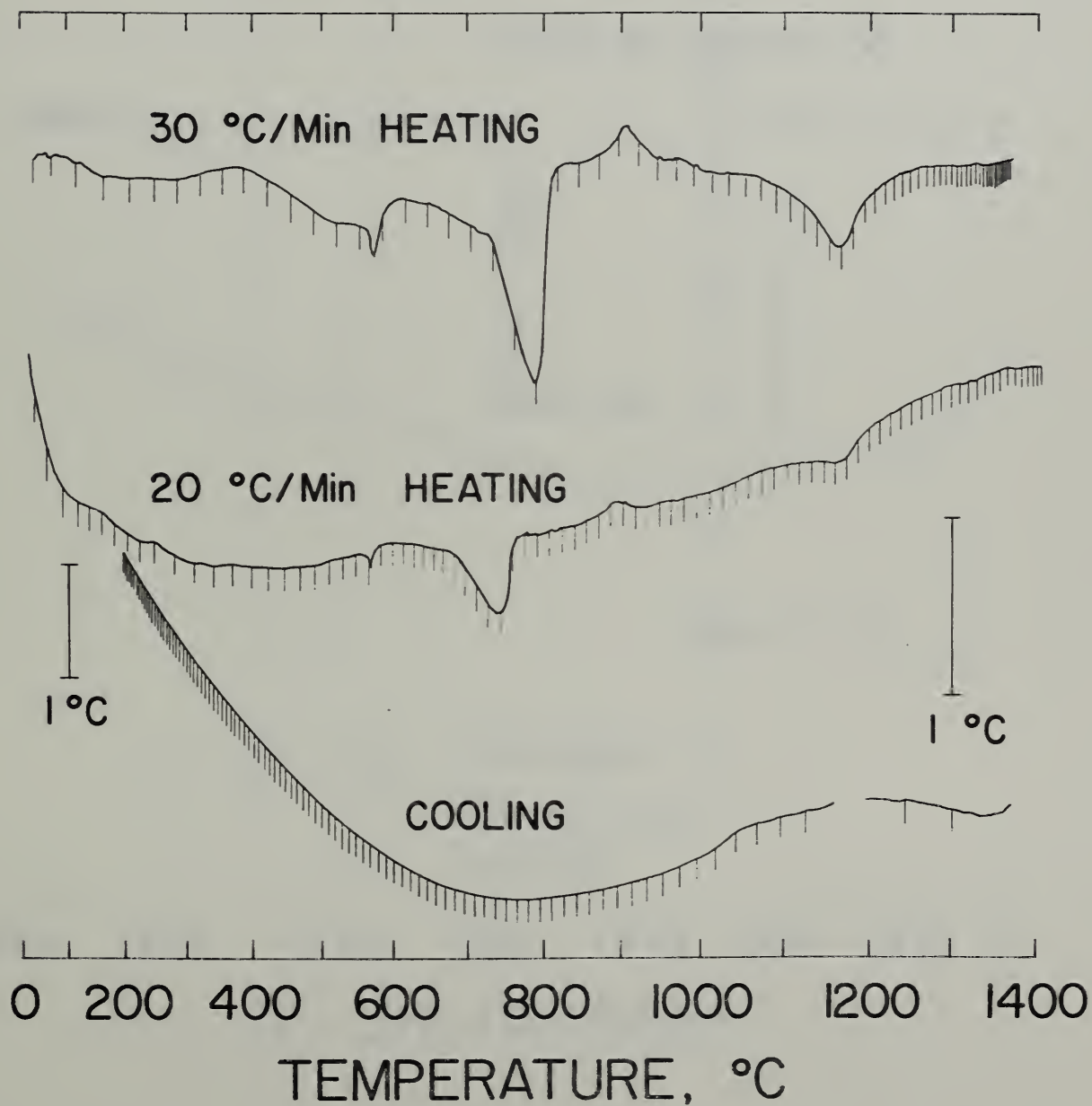
Figure 24 Differential thermal analyses of granitic detrital soil.

63
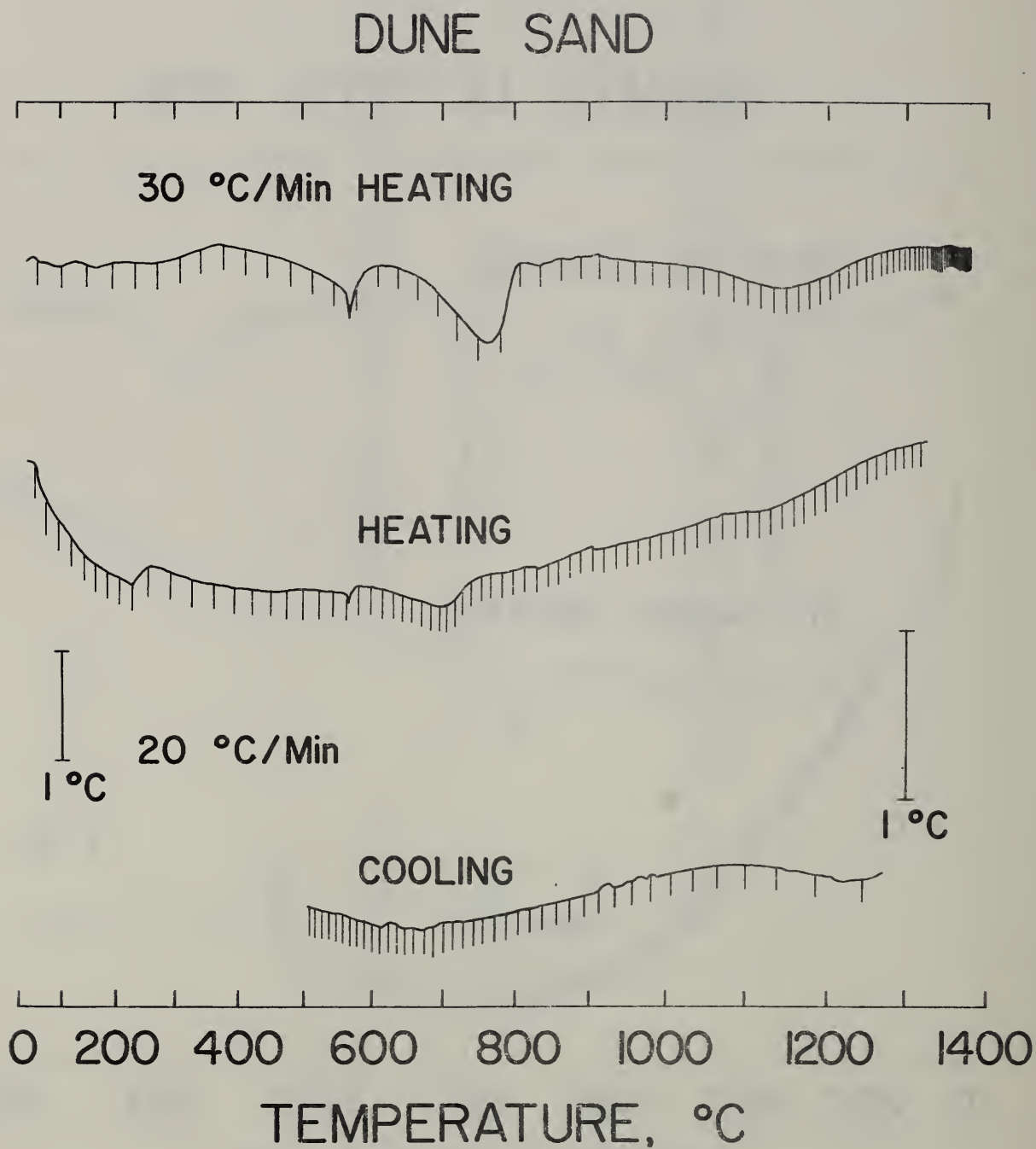
Figure 25 Thermogravimetric analysis of dune sand.
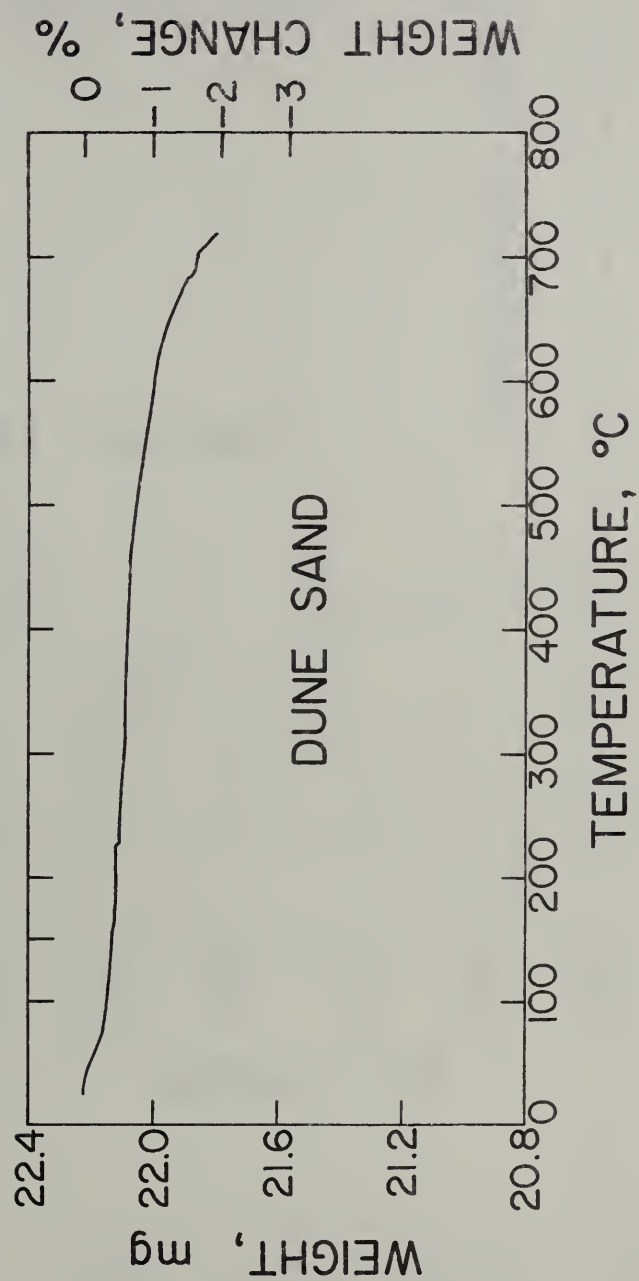
Figure 26 . Differential thermal analyses of dune sand.
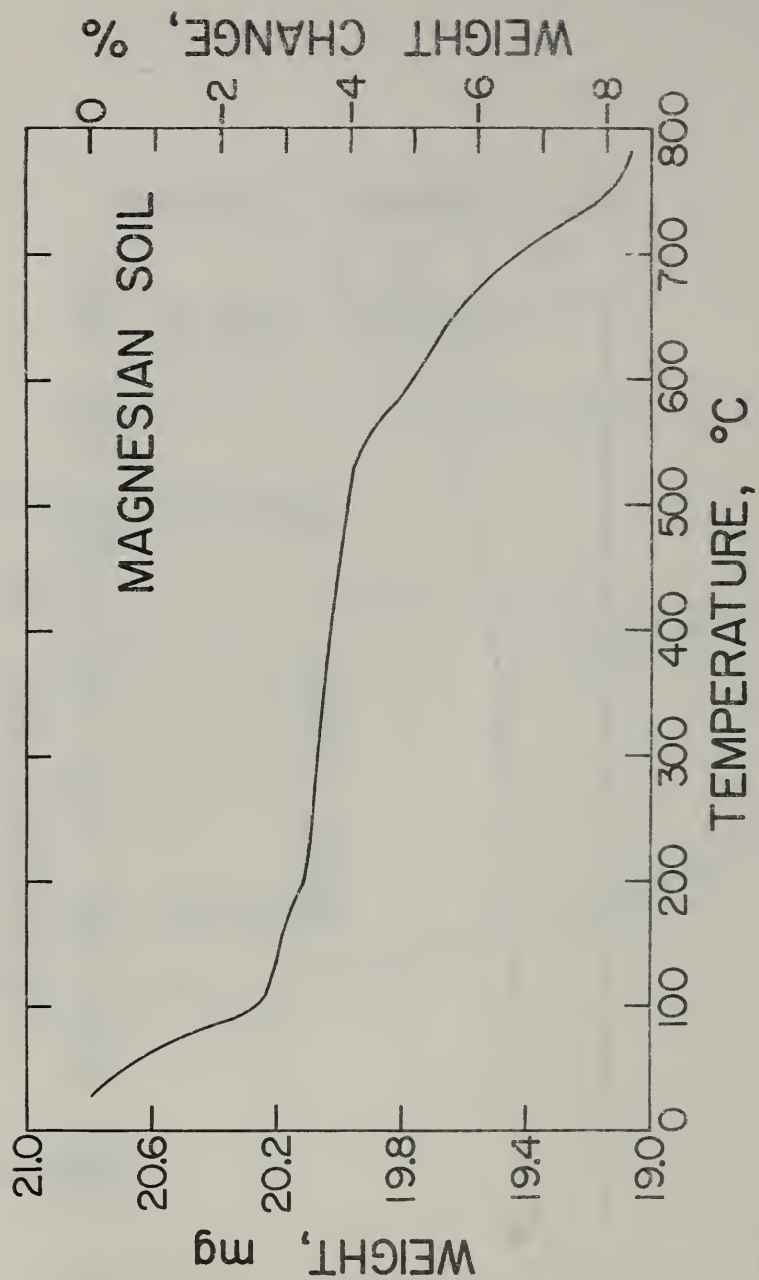
Figure 27. Thermogravimetric analysis of magnesian soil.

66

MAGNESIAN SOIL

30 °C/Min HEATING

1 °C

1 °C

0 200 400 600 800 1000 1200 1400

TEMPERATURE, °C
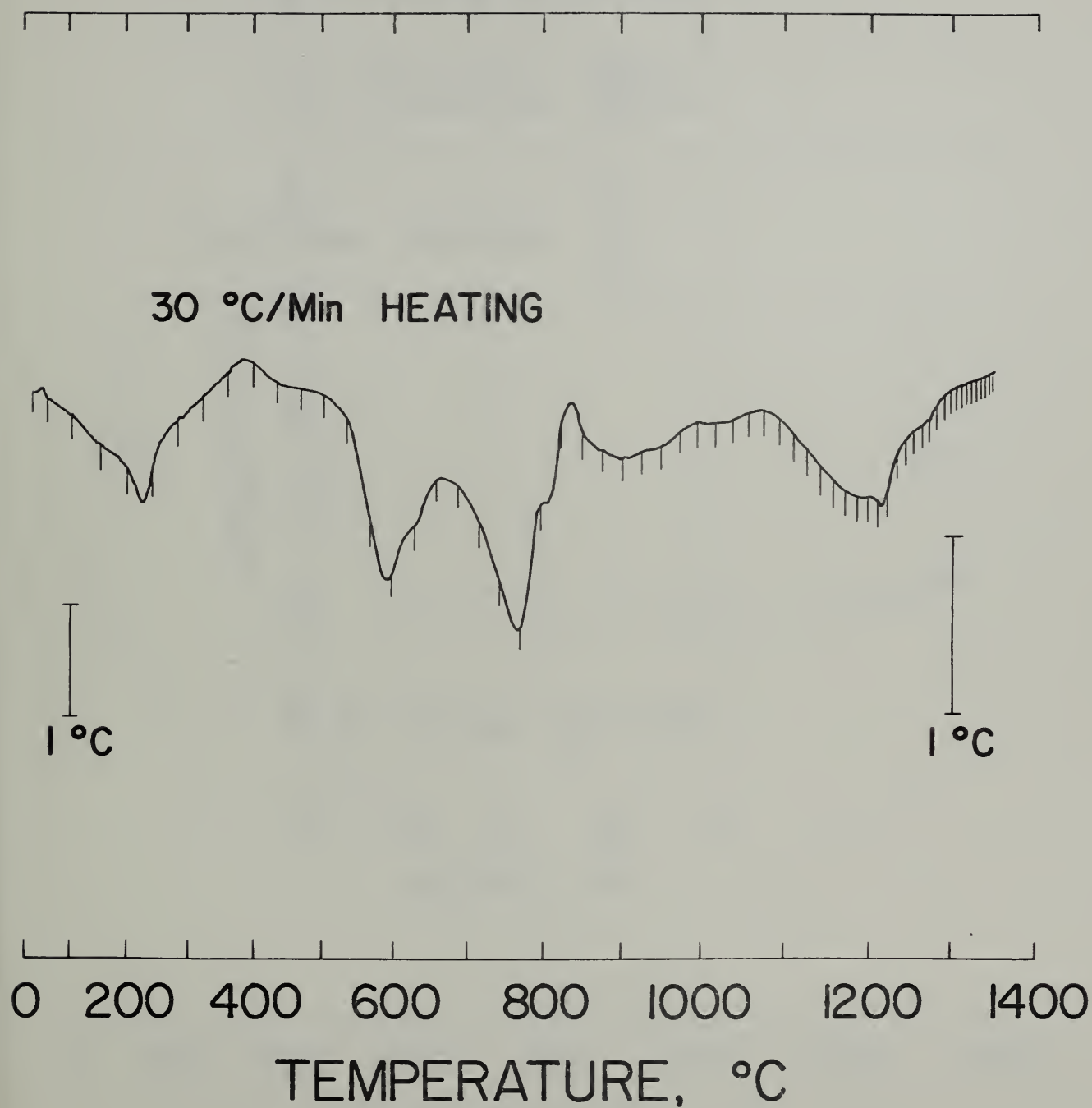
Figure 28. Differentil thermal analysesof magnesian soil.
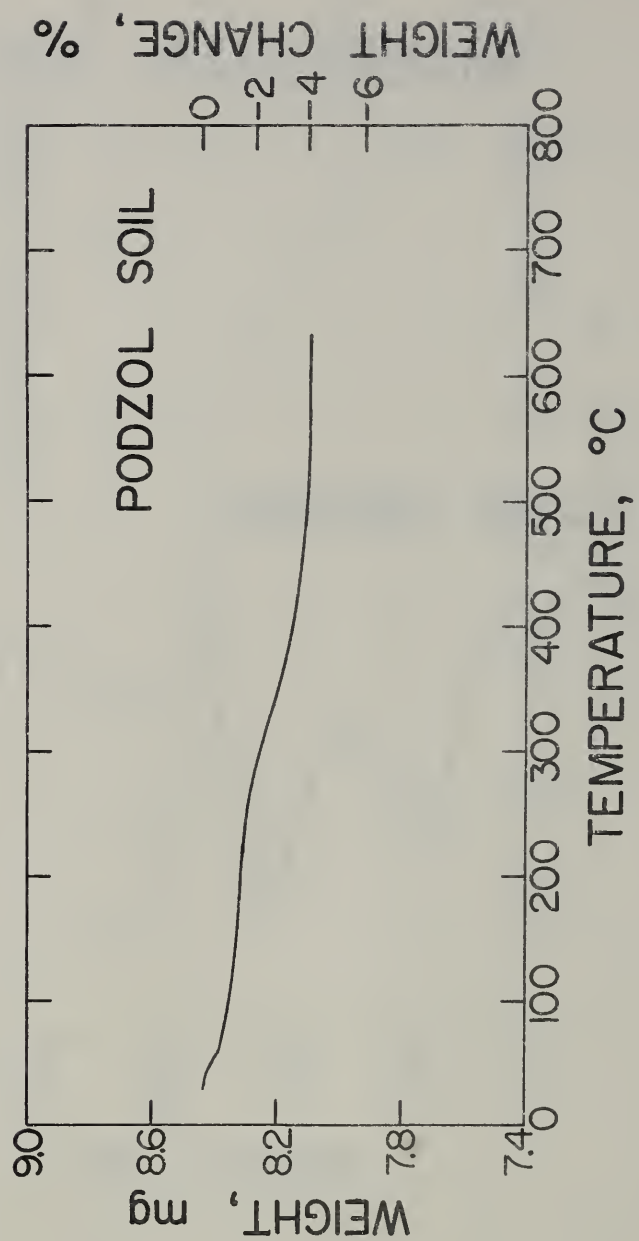
Figure 29. Thermogravimetric analysis of podzol soil.
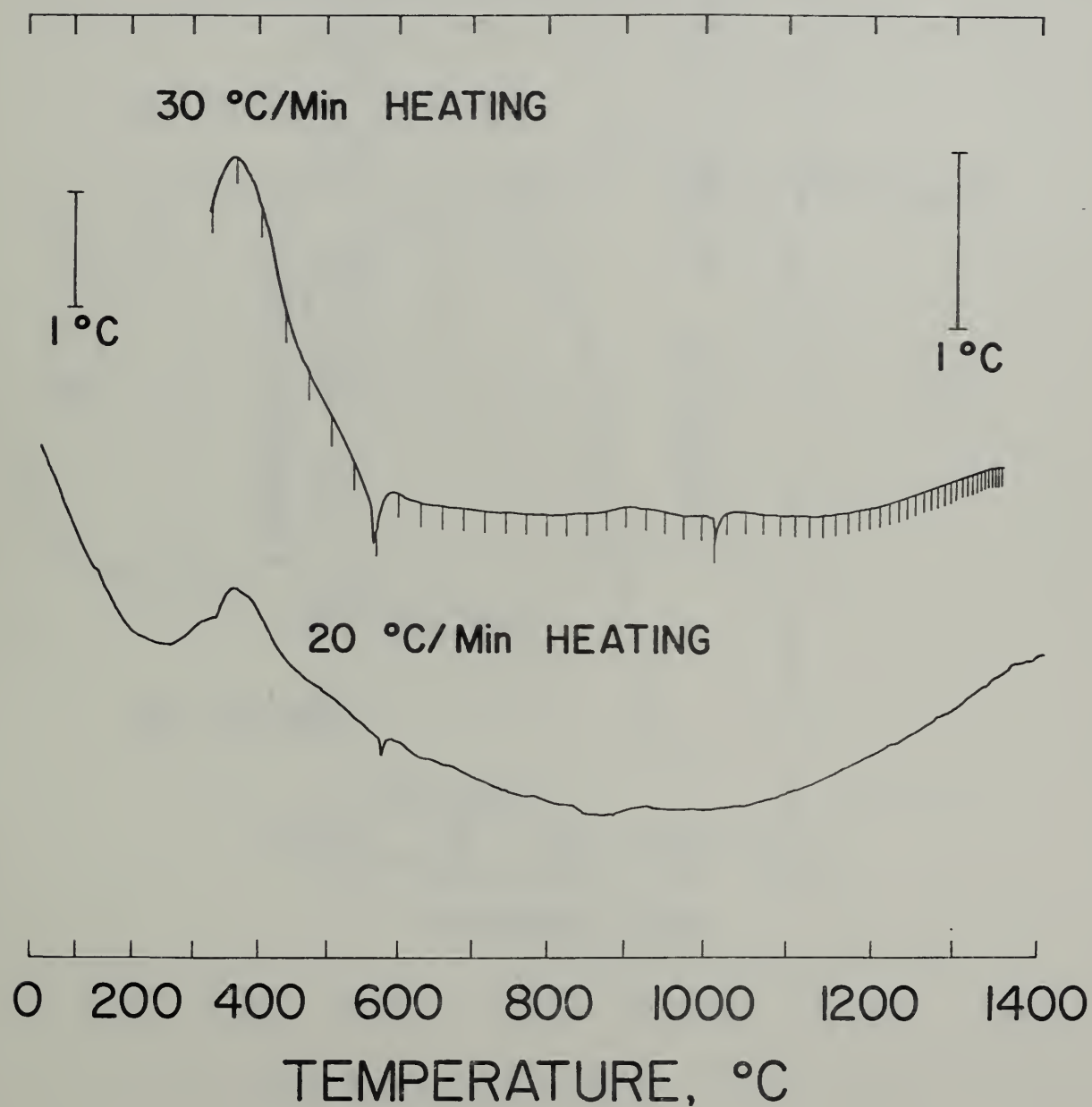
Figure 30. Differential thermal analyses of podzol soil.
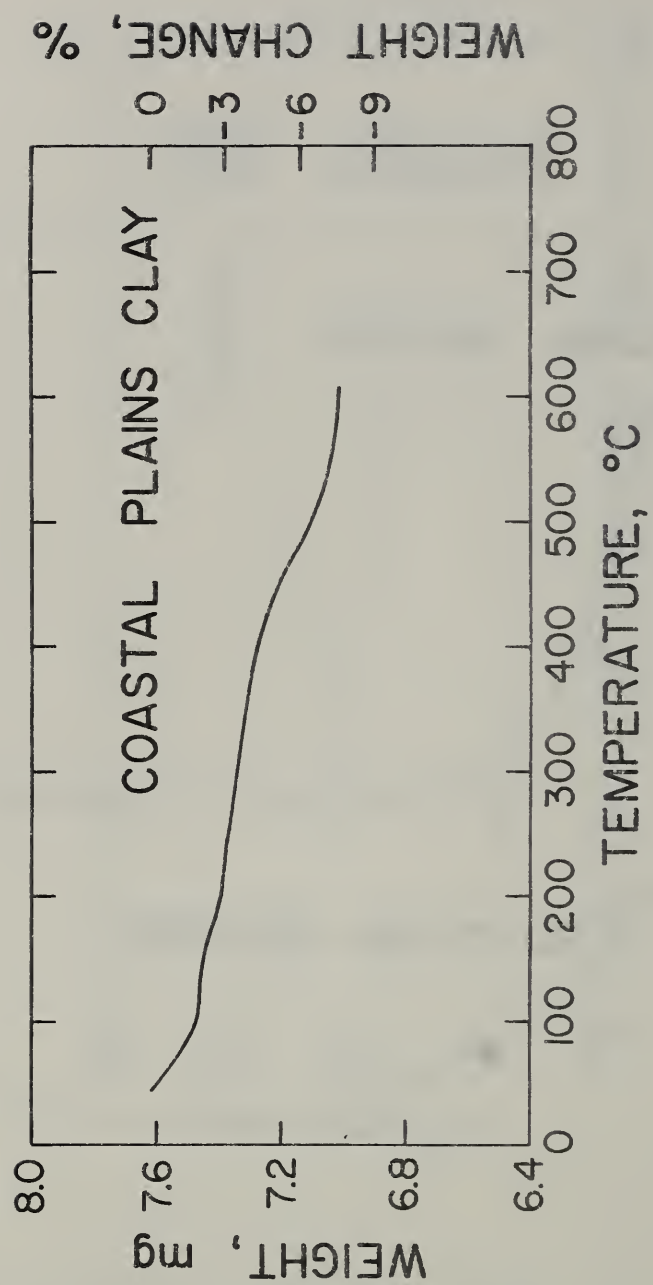
Figure 31. Thermogravimetric analysis of coastal plains clay.

70
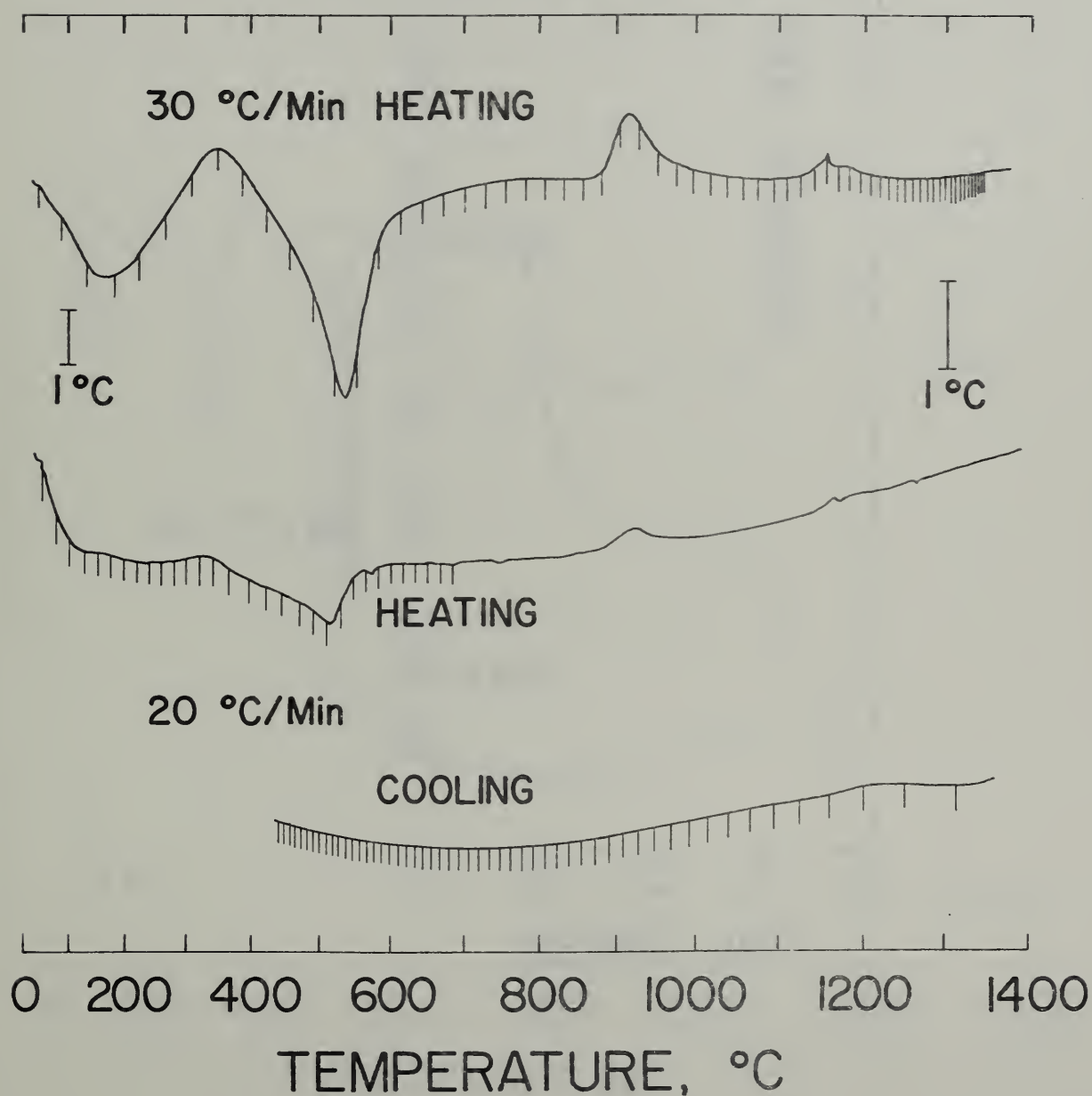
Figure 32. Differential thermal analyses of coastal plains clay.
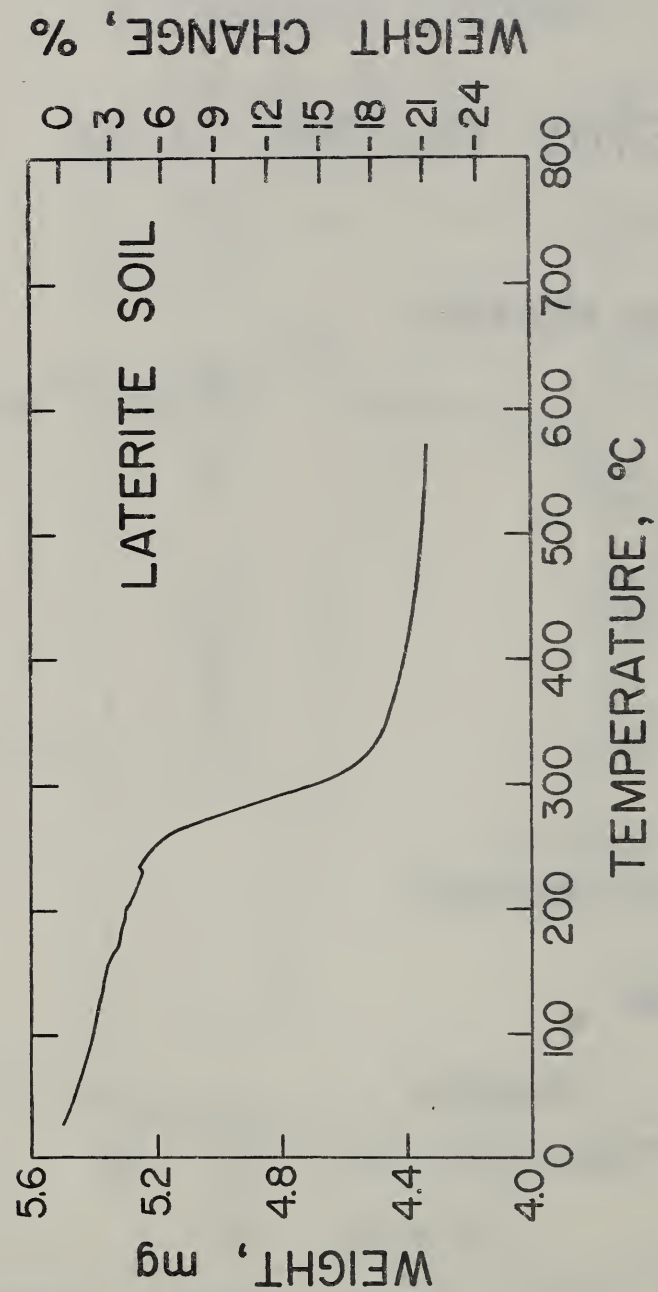
Figure 33. Thermogravimetric analysis of laterite soil.
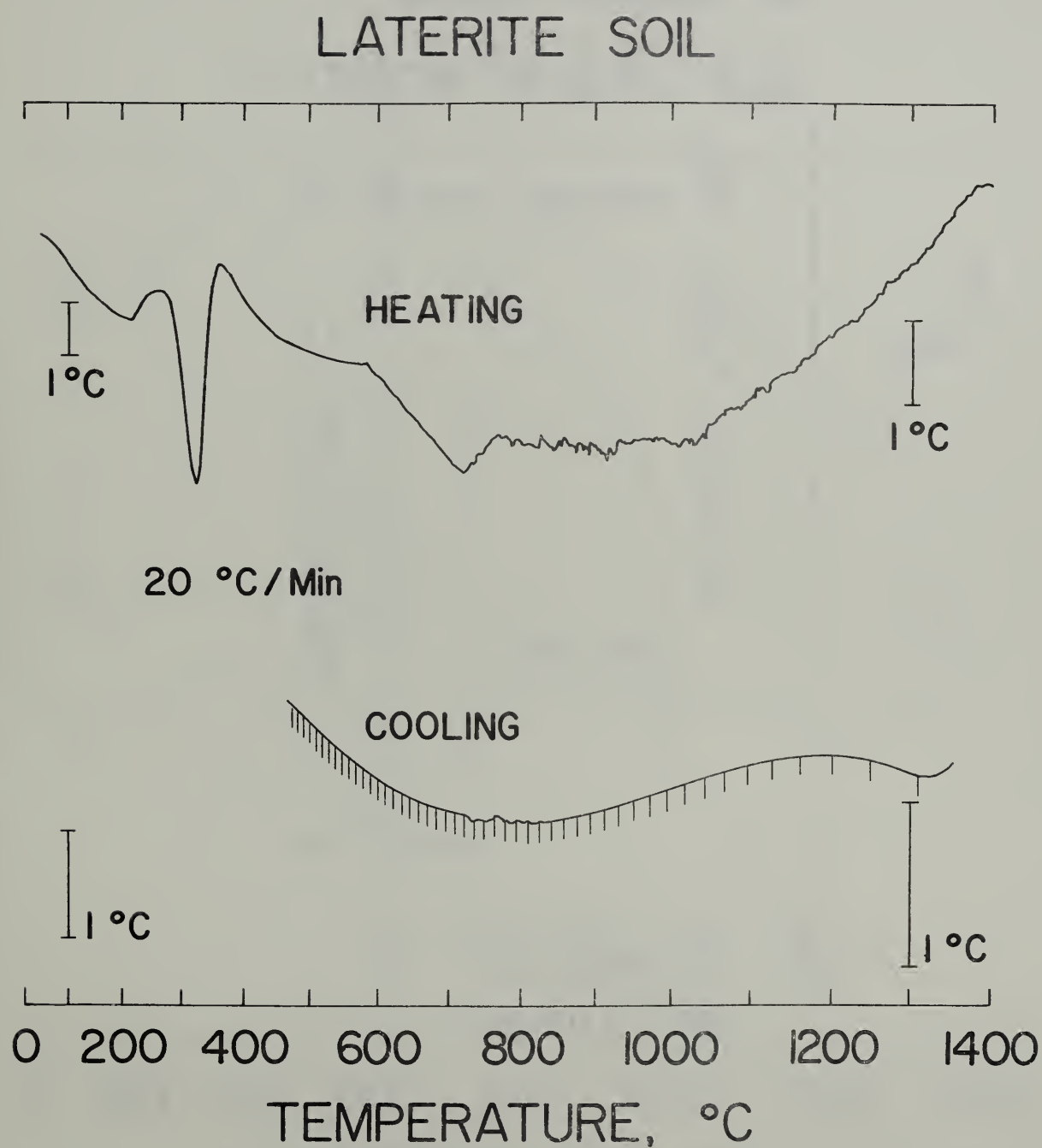
Figure 34. Differential thermal analyses of laterite soil.
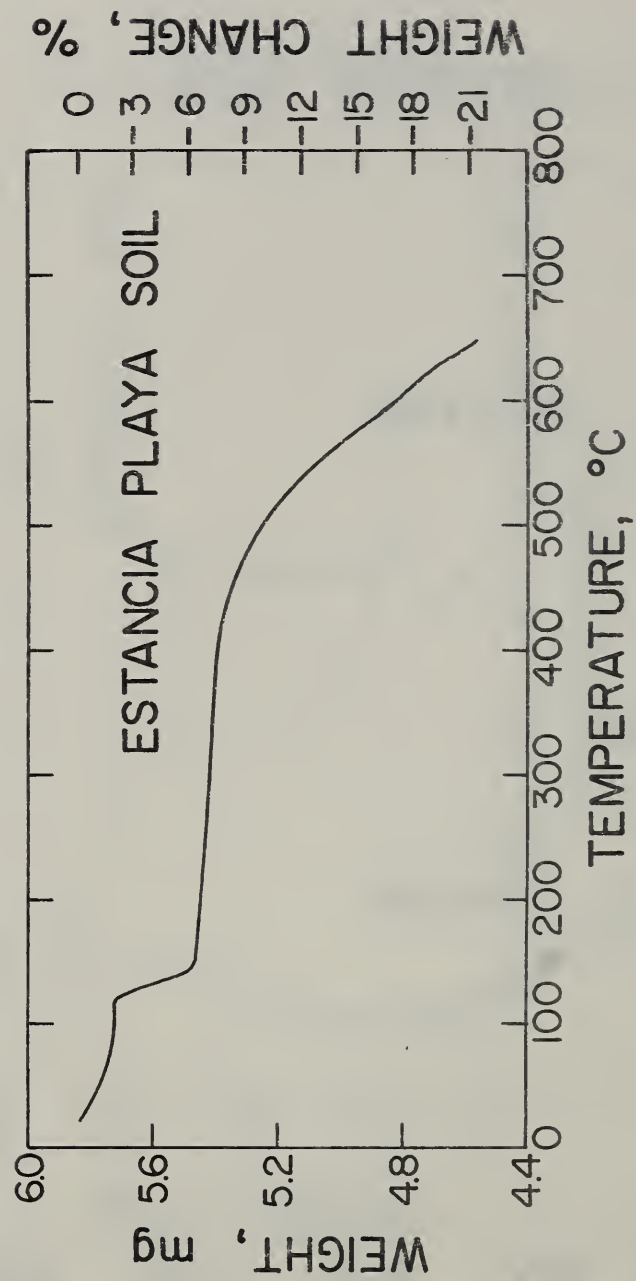
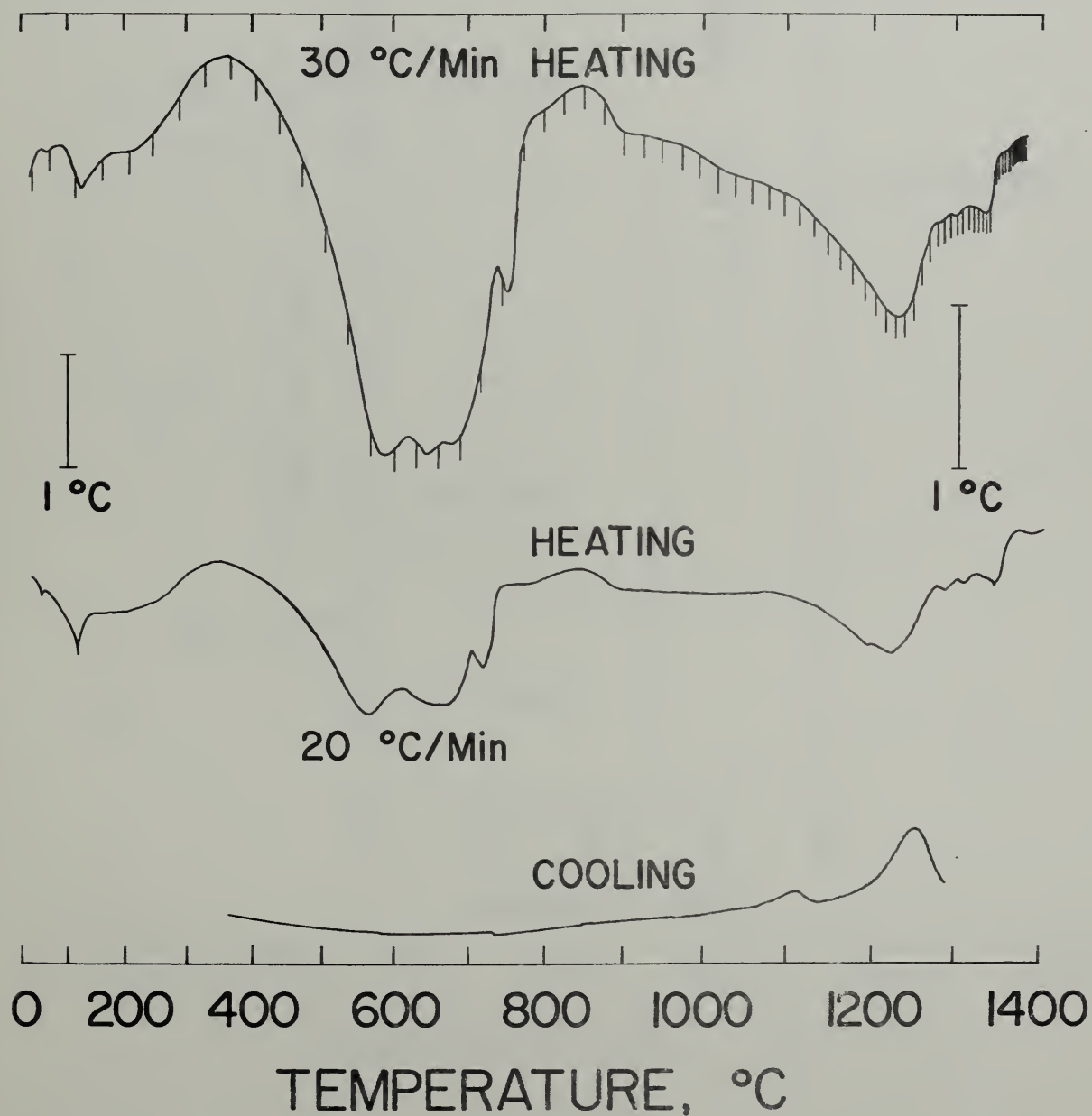Figure 35. Thermogravimetric analysis of estancia playa soil .

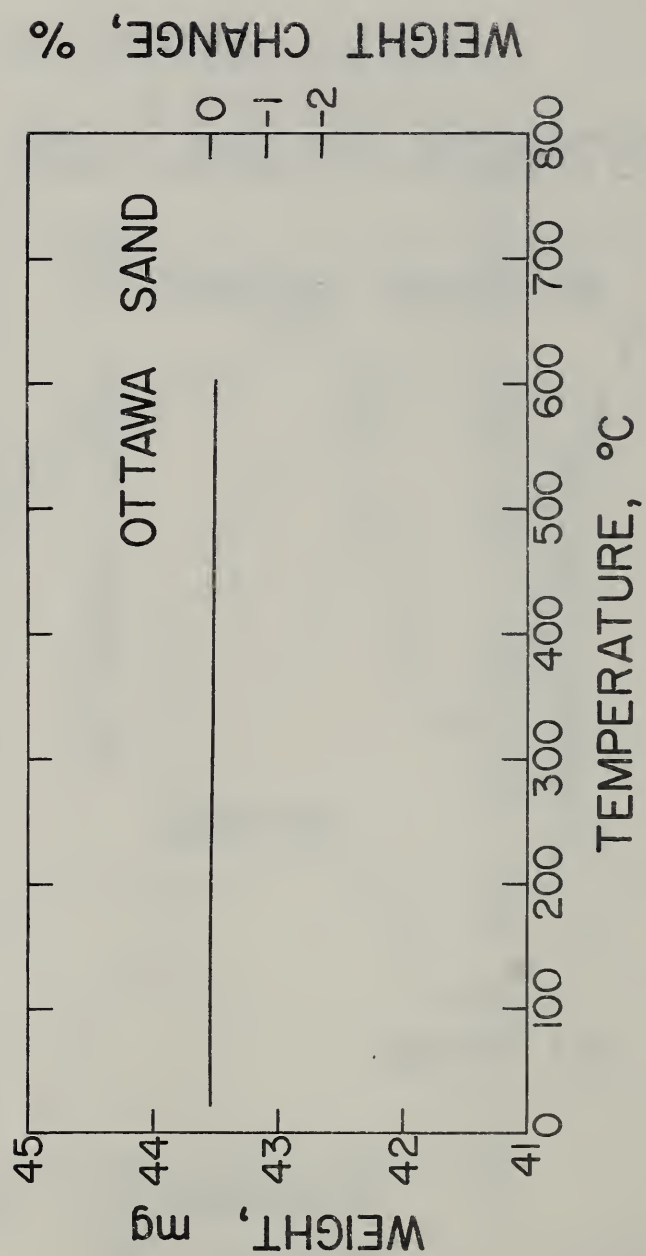Figure 36. Differential thermal analyses of estancia playa soil.
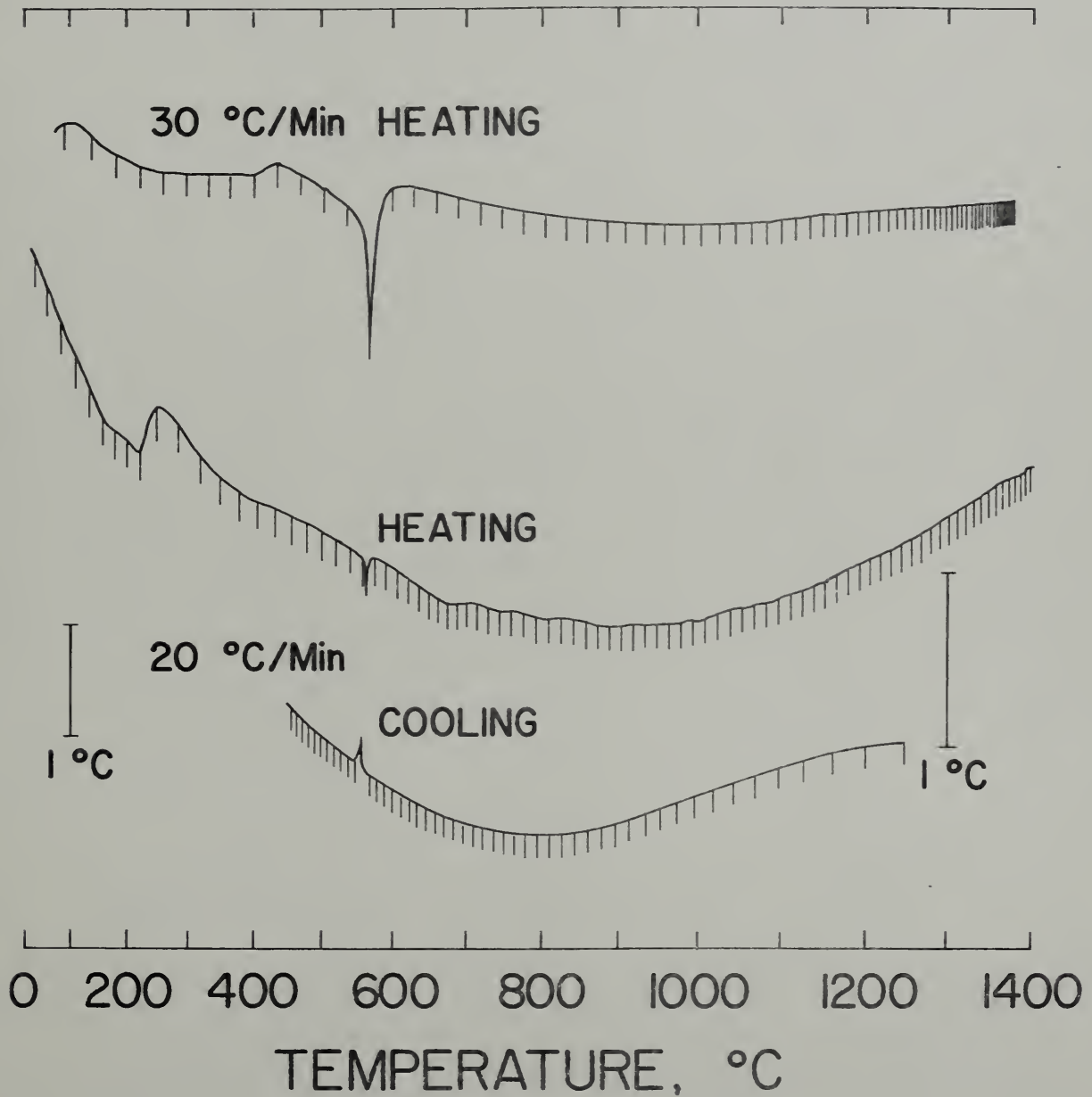
Figure 37. Thermogravimetric analysis of Ottawa sand.

Figure 38. Differential thermal analyses of Ottawa sand.